1 2  9 0

UNIVERSIDADE D
COIMBRA

Miguel Toste dos Santos Alves

Bubble Generation in Effervescent Atomization

Dissertation within the scope of the Master of Science in Mechanical Engineering, Energy and Environment supervised by Professor Miguel Rosa Oliveira Panão, Ph.D. and presented at the Department of Mechanical Engineering, University of Coimbra

February of 2023

FACULDADE DE CIÊNCIAS E TECNOLOGIA
UNIVERSIDADE D COIMBRA

Bubble Generation in Effervescent Atomization

Submitted in Partial Fulfilment of the Requirements for the Degree of Master of Science in Mechanical Engineering in the speciality of Energy and Environment

Geração de Bolhas em Atomização Efervescente

Author
Miguel Toste dos Santos Alves

Supervisor
Miguel Rosa Oliveira Panão, Ph.D.

Jury

President	Professor **José Joaquim da Costa, Ph.D.** Associate Professor, University of Coimbra
Supervisor	Professor **Miguel Rosa Oliveira Panão, Ph.D.** Assistant Professor, University of Coimbra
Vowel	Professor **Ana Sofia Oliveira Henriques Moita, Ph.D.** Assistant Professor, University of Lisboa

Institutional Collaboration

1 2 9 0 UNIVERSIDADE D COIMBRA
Universidade de Coimbra

Associação para o Desenvolvimento da Aerodinâmica Industrial

Coimbra, February, 2023

"Don't fear failure. Not failure, but low aim, is the crime. In great attempts it is glorious even to fail." - Bruce Lee

To my family and friends.

Acknowledgements

The accomplishment of this dissertation was only made possible thanks to the unconditional support of a few individuals to whom I dedicate a few words.

To my mentor, Miguel Panão, for his dedicated and indispensable support from the construction of the setup to image processing, whose algorithm development was only made possible thanks to his prior knowledge, for which he deserves credit.

To all my colleagues, and professors for all the constructive criticism which helped me improve academically and personally.

To all my friends for their support, laughs and good times during this journey.

To my sister Patrícia, and partner Diogo, for all the joy and positive support, and, especially, to the newborn Alexandre who was brought into this world on a very special day.

Saving the best for last, to my parents, Paula and Carlos, for all the love and understanding shown throughout my academic journey. Words cannot express my gratitude. Thank you.

Abstract

Effervescent atomization is a method of twin-fluid atomization that relies on introducing bubbles internally to aid in the overall process of producing a fine spray.

The purpose of an atomization method is to control the droplet size with the least energy input cost possible. According to the available literature, more than 90% of the total input energy is related to the pressurization and introduction of gas required to produce the desirable two-phase mixture. Therefore, in this dissertation it is studied the hypothesis of minimizing this component of energy, which would greatly improve atomization efficiency.

An experimental and theoretical study is presented on a new approach to generate bubbles in effervescent atomization. The main idea is to replace the mechanical aerator used to inject gas bubbles with local thermal-induced nucleate boiling to achieve a controlled bubbly flow generation, through a simple electronic system.

This work represents only the first step in evaluating this hypothesis. The experiments were conducted with Stagnated Liquid (SL), and were mainly to study the fundamental mechanisms involved in generating bubbles through local nucleate boiling on a thin wire, and compare the bubble generation morphology with the bubble characteristics in effervescent atomization. An experimental apparatus was constructed with an optical access window to visualize and capture, via a high-speed camera, the subcooled boiling process.

Several bubble phenomena were observed, which were also found in the literature. In experiments with $\Delta t = 1.67s$, the maximum bubble size reached was $560.52\mu m$ with a power input of $28.551W$. Furthermore, a bubble size cumulative distribution of $\Delta t = 1.67s$ tests is demonstrated.

A simple force balance analysis was made to test the applicability of this approach in effervescent atomization, considering the main forces acting on bubbles. The drag force exerted by the flowing liquid, when used in atomization, which will promote bubble departure, and the surface tension force between bubble-wire that will oppose its departure. An interesting relation between a parameter ϕ, which considers the ratio between the bubble's contact perimeter (l) with its diameter (D_b), and the capillary number (Ca) is presented.

In the future, continued work is necessary to test this different approach with Flowing Liquid (FL), as well as the use of multiple wires with different orientations and locations. Distilled water was used as the liquid.

Keywords: Effervescent atomization, Local nucleate boiling, Thin wire, Bubble characteristics

Resumo

Atomização efervescente é um método de atomização que recorre à utilização de um gás, injetado internamente em forma bolhas, que serve para auxiliar no processo de atomização.

O objetivo de um método de atomização é controlar o tamanho de gotas geradas com o mínimo custo de energia possível. De acordo com a literatura, mais de 90% da energia total necessária está relacionada com a pressurização e injeção do gás no líquido em escoamento, de forma a obter a mistura bifásica desejada. Nesta dissertação será estudada a hipótese de minimizar esta componente de energia que poderá melhorar substancialmente a eficiência de atomização.

É apresentado um estudo experimental e teórico sobre uma nova abordagem de geração de bolhas em atomização efervescente. A ideia principal é avaliar a possibilidade de substituir a forma de introdução do gás no líquido, através de um processo de ebulição nucleada local para produzir bolhas de forma controlada no interior do injetor, através de um sistema de controlo elétrico.

Este trabalho representa apenas o primeiro passo necessário para avaliar esta hipótese. As experiências realizadas, com fluido estagnado, têm como objetivo estudar os mecanismos fundamentais envolvidos na geração de bolhas através de ebulição nucleada local com a utilização de um fio fino, e comparar a morfologia de bolhas geradas com a literatura sobre atomização efervescente. A instalação criada e construída permite a visualização e captura, através de uma câmera de alta velocidade, deste processo.

Os vários fenómenos relacionados com o comportamento de bolhas em ebulição nucleada local encontrados na literatura foram observados durante os ensaios. Nos ensaios com uma duração de $\Delta t = 1.67s$, o tamanho máximo de bolha atingido foi $560.52\mu m$. Complementarmente, uma distribuição cumulativa do tamanho de bolha dos testes $\Delta t = 1.67s$ é demonstrada.

Uma análise de forças foi feita para testar a aplicabilidade desta abordagem em atomização efervescente, levando em consideração as principais forças que atuam sobre as bolhas. A força de arrasto exercida pelo líquido em escoamento num processo de atomização, que levará à sua libertação, e a força da tensão superficial entre bolha-fio, que se vai opor à sua libertação. É apresentada uma relação entre um parâmetro ϕ, que corresponde ao ratio entre o perímetro de bolha em contato com o fio (l) e o seu diâmetro (D_b), com o número de capilaridade (Ca).

Futuramente, será necessário testar esta hipótese com o líquido em movimento paralelamente com múltiplos fios com diferentes orientações e posições. Água destilada foi o líquido usado neste estudo.

Palavras Chave: Atomização efervescente, Ebulição nucleada local, Fio fino, Caraterísticas das bolhas

Contents

Nomenclature

A_d	Total surface area of droplets $[m^2]$
A_L	Total surface area of the initial bulk liquid $[m^2]$
A	Area $[m^2]$
D	Diameter $[\mu m]$
D_{32}	Sauter Mean Diameter $[\mu m]$
E_a	Interfacial energy required for atomization [J]
e_a	Interfacial surface energy[J/kg]
E_i	Input energy available for atomization [J]
e_i	Input energy[J/kg]
F_B	Buoyancy force [N]
F_D	Liquid drag force [N]
F_I	Bubble inertia force [N]
F_M	Gas momentum flux [N]
F_M	Marangoni force [N]
F_S	Surface tension force [N]
g	Gravitational acceleration $[m/s^2]$
i	Current [A]
l	Bubble attachment characteristic length $[\mu m]$
$\dot{m}$	Mass flow rate [kg/s]
m	Mass [kg]
P	Power [W]
p	Pressure [Pa]
q''	Heat flux $[W/m^{-2}]$

R	Resistance [Ω]
T	Temperature [$^{\circ}C$]
t	Time [s]
U	Velocity [m/s]
$\dot{V}$	Volume flow rate [m^3/s]

Dimensionless Numbers

c_D	Drag Coefficient
Ca	Capillary number
Re	Reynolds Number
We	Weber number

Greek Symbols

η_a	Atomization efficiency [%]
ϕ	$= l/D_b$ [-]
ρ	Density [kg/m^3]
σ	Surface tension [N/m]

Subscripts

∞	Ambient
b	Bubble
d	droplet
eff	Effective
G	Gas
inj	Injection
L	Liquid
sat	Saturated
W	wire

List of Figures

List of Tables

List of Abbreviations and Acronyms

BGV Bubble Growth Velocity

BSD Bubble Size Distribution

FL Flowing Liquid

FPS Frames per Second

GLR Gas to Liquid Ratio

NiCr Nickel-Chromium

PETG Polyethylene Terephthalate Glycol

SL Stagnated Liquid

SMD Sauter Mean Diameter

1. Introduction

Atomization is a process designed to produce droplets from a liquid bulk and there is a variety of strategies used for atomization. The current dissertation focuses on effervescent atomization, considered within the air-assist category (although gas-assist is the most appropriate generic term used henceforth), where the two-phase mixture generated internally in the atomizer before the exit orifice facilitates liquid breakup into droplets.

Effervescent atomization has shown to have immense potential. Its advantages are – the capability to atomize highly viscous liquids; the use of lower injection pressures; larger exit orifice diameters, reducing the manufacturing cost, clogging, and erosion; lower pollutant emissions when using air to assist atomization; and the possibility of controlling droplet size. Effervescent atomization rose in popularity among researchers due to the significant improvements in performance in terms of smaller drop sizes ($\mathcal{O}(D_d) \sim 10\,\mu m$), requiring lower injection pressures when compared to other methods of twin-fluid atomization. Moreover, the advantages include high efficiency, economy, and environmental protection over conventional pressure and pneumatic atomizers.

The transfer of surface energy dominates the liquid atomization process. Namely, the ratio between the interfacial surface energy used to produce droplets (e_a) and the input energy (e_i) required to produce the two-phase mixture is defined by the atomization efficiency for gas-assisted sprays. According to Panão [2021], in the atomization efficiency, the general relation for the energy required for atomization is

$$e_a[J/kg] = \left(\frac{\sigma_L}{\rho_L}\right)\left[\frac{6}{D_{32}} - \frac{1}{L_c}\right] \tag{1.1}$$

with σ_L and ρ_L as the atomizing liquid surface tension and density, respectively, D_{32} is the Sauter Mean Diameter (SMD) or the area-weighted mean diameter, and L_c is a characteristic length of bulk liquid before atomization. Regarding effervescent sprays, Jedelsky and Jicha [2014] formulated the input work to pressurize the liquid and add gas as

$$e_i[J/kg] = \frac{p_L}{\rho_L} + GLR \cdot \rho_G(p_\infty + p_G)\ln\left(1 + p_G/p_\infty\right) \tag{1.2}$$

with $p_L,\ p_G,\ p_\infty$ as the liquid, gas, and ambient pressure, respectively, ρ_G is the gas density, and $GLR = m_G/m_L$ is the Gas-to-Liquid-Ratio. A simple scale analysis indicates the scales for the atomization efficiency in this strategy range between $0.01 - 1\%$, with the input work necessary to add gas representing more than 90% of the input energy. One of the key features of this atomization strategy is reducing the work necessary to pressurize the liquid and produce small droplets, compared to other strategies without gas-assisting, but the price paid is the energy cost of adding gas to produce bubbly flows at the nozzle exit.

1.1. Motivation and Objectives

The present dissertation's motivation is the hypothesis that using an electronically controlled bubble generation system might reduce the input energy required to produce the gas-assisting liquid breakup in effervescent atomization. However, the first research stage, and the main objective, would be to investigate bubble generation timescales under SL. Therefore, the specific objective in this dissertation are:

1. Design and build an experimental setup to produce local nucleate boiling events using a 100µm in diameter Nickel-Chromium (NiCr) wire, similar to the approach of Nukyiama experiment [Nukiyama, 1966]. The installation apparatus has optical access to visualize and capture, with a high-speed camera, the bubble generation process.

2. Analyze bubble morphology for a range of supplied power. A comparison is made with the bubble characteristics in effervescent atomization and subcooled boiling literature.

3. Characterize the bubble growth rate retrieved from a developed image processing algorithm in Matlab to evaluate bubble formation timescales.

It is noteworthy to clarify that this study is only the first of several steps to validate the possibility of generating thermal-induced bubbles inside an atomizer to produce effervescence instead of using work to add gaseous bubbles, increasing the input energy.

1.2. Literature Review

Atomization is a process that transforms a bulk liquid into individual droplets forming a spray. The transformation of liquid occurs in two major stages: in the primary stage, the bulk liquid breaks into ligaments and droplets; in the second stage, the ligaments and larger droplets further break into smaller droplets. The second stage of liquid atomization only occurs in certain aerodynamic conditions. Fig. 1.1 includes more detailed stages of the atomization process.

The applications of sprays include several different fields, such as coating, spray drying, agricultural applications, paint spraying, power generation, and many others. In some applications, such as combustion, one benefits from producing smaller droplets. Still, in other applications, such as paint spraying and agricultural sprays, below a certain size, the interaction of droplets with secondary flows in the surrounding environment can stop them from reaching the intended surface. Therefore, building atomizers capable of controlling drop size is an engineering challenge.

The purpose of an atomization strategy is to control the production of drop sizes with the least energy input. The simplest atomizers are pressure-driven and cheap to manufacture, using pressure energy to convert the liquid into droplets due to the large pressure differential at the nozzle exit. Diesel injectors and Gasoline-Direct Injectors are common examples. However, as formulated in Eq. (1.1), this strategy implies using large input energy values, lowering the atomization efficiency. Twin-fluid atomizers which consist of gas-assist and airblast atomizers have similar methods, with the main difference being that one uses relatively small quantities of gas at high velocities (air-assist) and the other employs substantial amounts of gas at lower velocities (airblast). In air-assist atomizers, the mixing of liquid-gas can be internal, inside the atomizer

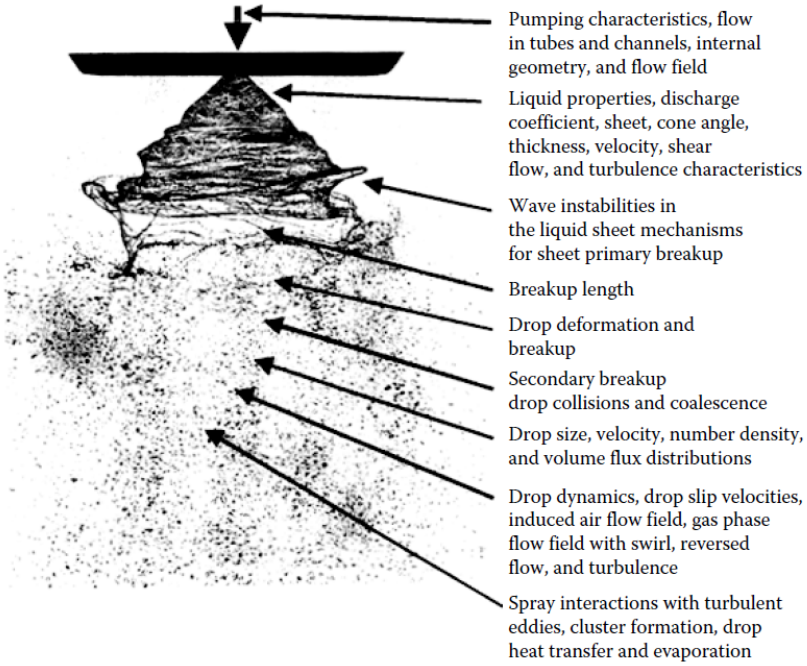

Figure 1.1: Example of the multitude of stages forming a spray [Lefebvre and McDonell, 2017].

before the exit nozzle, or external, where the gas impinges on the liquid outside of the discharge orifice. Other types of atomizers are not as common as the ones aforementioned, e.g., Electrostatic and Ultrasonic. In Fig 1.2 it is shown several types of atomizers.

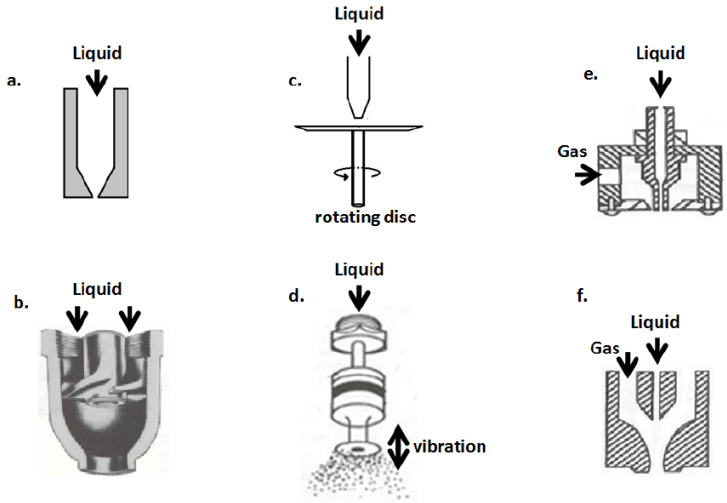

Figure 1.2: Several types of atomizers (a) Pressure, (b) Pressure-swirl, (c) Rotary, (d) Ultrasonic, (e) Twin-fluid: external mixing, (f) Twin-fluid: internal mixing [Shepard, 2011].

Jedelsky and Jicha [2014] showed that only a small portion of the input work represents the surface energy used in atomization. Most of the input energy is lost due to the friction from the nozzle inlet until its exit, in the necessary kinetic energy transported by the liquid and gas. In the case of twin-fluid atomizers, the gas-liquid interaction also uses a certain amount of input energy. Other energy losses are associated with

thermal, acoustic, etc. Therefore, when defining the atomization efficiency as the ratio between interfacial energy required to atomize the liquid, $E_a[J]$, and the input energy available for atomization, $E_i[J]$:

$$\eta_a = \frac{E_a}{E_i} \tag{1.3}$$

each term depends on the liquid atomization strategy used.

In the available literature, almost all works consider the SMD as the most appropriate mean diameter used in the atomization efficiency formulation but fail to explain the reason. SMD (or D_{32}) represents the volume-to-surface area of the spray using the diameter of each individual spray droplet, D_i, or the mean diameter of an area-weighted drop size distribution as clarified by Sowa [1992].

$$\text{SMD}[\mu m] = \frac{\sum D_i^3}{\sum D_i^2} \tag{1.4}$$

The interfacial energy required for atomizing the liquid is based on the variation between the total surface area of all droplets in the produced spray A_d and the total surface area of the initial bulk liquid A_L. Panão [2021] work showed the link between spray droplets interfacial energy and the SMD by observing from a mass balance that

$$A_d = \frac{6m_d}{\rho_L D_{32}} \tag{1.5}$$

where m_d is the mass of all droplets in the spray and ρ_L is the liquid density. In general terms, the total surface area of the initial bulk liquid A_L is given by

$$A_L = \frac{m_L}{\rho_L L_c} \tag{1.6}$$

where m_L is the mass and L_c is the characteristic length of the initial bulk liquid. Assuming $m_d = m_L$,

$$E_a = \sigma_L(A_d - A_L) = \frac{\sigma_L}{\rho_L} m_L \left(\frac{6}{D_{32}} - \frac{1}{L_c}\right) \tag{1.7}$$

with σ_L as liquid surface tension. Summarizing, the atomization efficiency (η_a) is:

$$\eta_a = \frac{\sigma_L}{\rho_L}\frac{m_L}{E_i}\left(\frac{6}{D_{32}} - \frac{1}{L_c}\right) \tag{1.8}$$

Interpreting Eq. (1.8), it is possible to increase the efficiency of liquid atomization by changing the values of the parameters involved in this expression. For example, lowering D_{32} for the same m_L from a larger L_c would result in an increase in efficiency. Or keeping the D_{32} low using a lower E_i, which would depend on the type and atomization method, and the kind of improvement investigated in this dissertation for Effervescent Atomization.

1.2.1. Effervescent atomization background

In the last three decades, much work has been done toward an internal mixing twin-fluid atomizer that uses the strategy of effervescent atomization [Cejpek et al., 2023,

Thiebes et al., 2022, Xie et al., 2022, Zhao et al., 2019]. This atomization strategy was first introduced by Lefebvre et al. [1988] in the 1980s, where it was formally described as 'aerated liquid atomization'.

In effervescent atomization, the gas is injected into the flowing liquid at low velocity before the exit orifice, producing a two-phase bubbly mixture inside the atomizer. Fig. 1.3 shows a typical effervescent atomizer design consisting of five main components: (1) the liquid and (2) gas supply ports, (3) a mixing chamber, (4) a perforated aerator tube, and (5) an exit orifice.

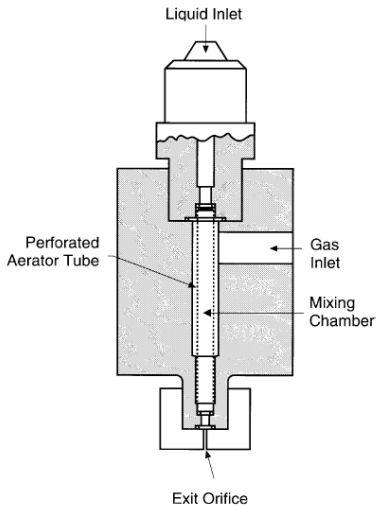

Figure 1.3: Typical structure of an effervescent atomizer [Sovani et al., 2001].

There are two main designs of this type: outside-in, represented in Fig. 1.3, or inside-out, which is done simply by switching the liquid and gas supply ports with little variations in design. According to Sovani et al. [2001], a typical effervescent atomizer is around $100mm$ long with $50mm$ of diameter, has a mixing chamber diameter between $5 - 25mm$, and exit orifices around $0.1 - 2.5mm$.

Fig. 1.3 shows where the liquid enters at the top of the atomizer and flows through the mixing chamber, where the gas with slightly higher pressure is introduced via a perforated aerator tube, leading to the exit orifice. At the nozzle exit, the abrupt pressure drop causes an 'explosive effect' on the two-phase mixture, which generates the fine spray. In this technique, the gas occupies most of the exit nozzle cross-sectional area since the gas has a lower density than the liquid, and this density difference causes the burst effect when the gas bubbles leave the nozzle, additionally to the pressure drop, helping to further breakup the liquid into droplets. This technique relies on bubble expansion.

In the gas-assist atomizer, the Gas to Liquid Ratio (GLR) has a considerable effect on the spray produced and bubble size [Rahman et al., 2012, Sun et al., 2018, 2019]. In the case of effervescent atomization, Jedelsky and Jicha [2013] implied that the overall surface area of the initial bulk liquid is much smaller than the total surface area of all droplets produced, which leads to a characteristic length at least one order of magnitude above D_{32}. Neglecting L_c, as Jedelsky and Jicha [2013] suggested, Panão [2021] shows the expression for the atomization efficiency in effervescent sprays, in terms of pressure, as:

$$\eta_a = \frac{6\sigma_L/D_{32}}{p_L + p_G} = \frac{6\sigma_L/D_{32}}{p_L + [GLR \cdot \rho^* p_\infty (1 + p_G^*) \ln(1 + p_G^*)]} \tag{1.9}$$

with $\rho^* = \rho_G/\rho_L$ and $p_G^* = p_G/p_\infty$. A scale analysis results in atomization efficiency values similar to other methods, still lower than 1%. However, since the different regimes change the behavior of bubbles in the fluid flow, it is not certain nor confirmed the hypothesis suggested in Jedelsky and Jicha [2013] unless the authors only reached the bubbly flow regime with tiny bubbles mixed in the liquid.

1.2.2. Internal two-phase flow: Effervescent atomization

In an effervescent atomizer one can potentially observe three regimes of internal flow: bubbly, slug, and annular regime (represented in Fig. 1.4). The bubbly flow regime is easily achieved and it is composed by a large number of small bubbles dispersed in the flow . Further increase in GLR will result in the formation of larger bubbles that will eventually collide, due to coalescence, transitioning to the slug regime. The slug regime is a combination of bubbles larger than the ones found in the bubbly flow and large gas pockets that usually vary in shape and size. Raising the GLR even more will lead to the annular regime, which is, simply said, a core flow of gas surrounded by the liquid with the annular shape.

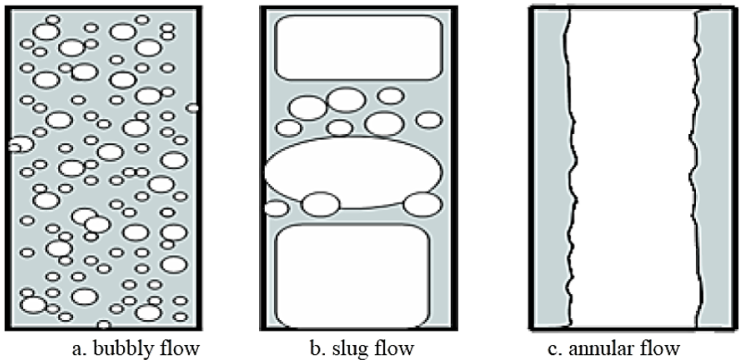

Figure 1.4: Flow regimes inside an effervescent atomizer [Shepard, 2011].

The internal flow regime it is said to be mostly dependent on GLR, however the transition from one regime to another can be affected by the liquid and gas proprieties and injection pressures as well as the internal geometry.

Identifying the internal flow in effervescent atomizers have shown to be quite important, since the flow regime has a strong influence on the spray performance, as shown by Sun et al. [2018]. Bubble generation and bubble dynamics is what determines the flow regime.

In research studies it is reported that from spray stability point of view, effervescent atomization may be improved when operating in the bubbly regime. In the slug regime, spray stability is decreased due to the large pockets of gas followed by large pockets of liquid which result in a somewhat intermittent spray.

1.2.3. Bubble Characteristics: Effervescent Atomization

Bubble characteristics is considered primarily by their size and shape (bubble morphology) and velocity and flux (bubble dynamics).

In the past available literature, many researchers disregard the impact of bubble size in effervescent atomization, however the effects of this variable its increasingly being more analysed.

Bubble models normally assume that the bubble formed/introduced are roughly of spherical shape. On the other hand, others considered as a variation between spherical and ellipsoidal shape for one that seeks more accurate finds, specially at the gas injection ports. To simplify, considering all bubbles of spherical shape in the bubbly flow regime, seems quite a reasonable assumption for this study.

The bubble typical size in effervescent atomization literature varies from the study to study. The data available is dependent on the geometry and operating conditions conducted in that specific experiment. However, all studies have similar bubble diameter in terms of orders of magnitude, between $\mathcal{O}(10^{-3})$ and $\mathcal{O}(10^{-4})$ meters. Table 1.1 shows the representative, not the full representation, of the bubble size in effervescent atomization.

$D_{b,mean}$ [mm]	$D_{b,min}$ [mm]	$D_{b,max}$ [mm]
0.2 - 1.7	0.1 - 0.42	0.75 - 2.57

Table 1.1: Representative bubble size ($D_{b,mean}$, $D_{b,min}$, $D_{b,max}$) in effervescent atomization. Values extracted from [Rahman et al., 2012, Shepard, 2011, Sun et al., 2019].

Bubble Size Distribution (BSD) vary significantly in the literature. The work done by Sun et al. [2019] shows the BSD for a range of GLR with a liquid flow rate $13.89 g/s$. Fig. 1.5 shows the bubble size distribution of this experiment for different GLR (from 0.07% to 0.42%).

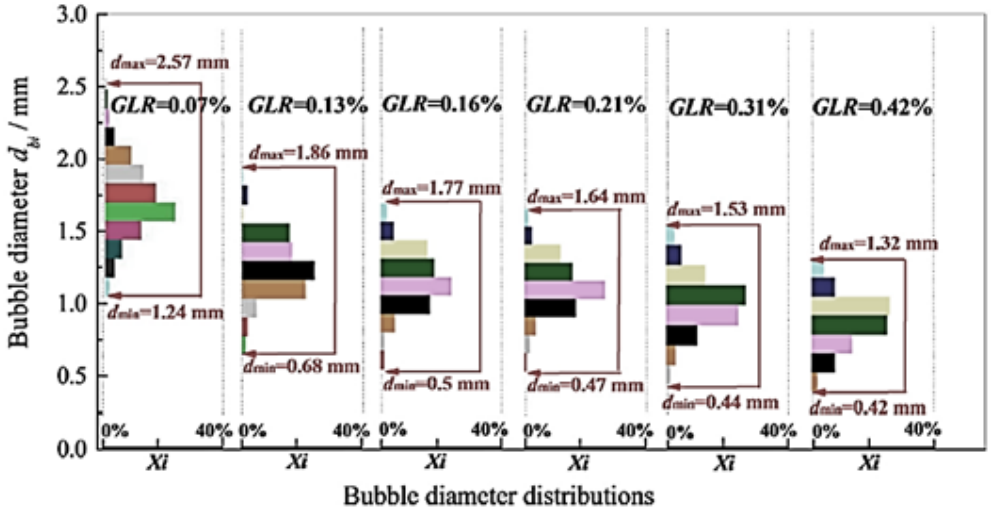

Figure 1.5: Bubble size distribution variation with GLR [Sun et al., 2019].

It is clear to see that GLR has a considerable effect on Bubble diameter. The maximum bubble size dropped to almost half between 0.07% and 0.42%.

Moreover, Rahman et al. [2012] presented the bubble maximum diameter, $D_{b,max}$ theoretical and experimental, as well as the minimum and mean bubble diameter obtained experimentally varying GLR. In Rahman et al. study, one of the theoretical maximum bubble diameters was calculated using Eq. 1.10 [from Hibiki et al. [2004]]. This equation is one of many proposed to estimate the maximum bubble size in the two-phase mixture. Others consider parameters, such as the critical value of Weber and the turbulent energy dissipation.

$$D_{b,max} = \frac{4\sigma^{0.5}}{g^{0.5}(\rho_L - \rho_G)^{0.5}} \tag{1.10}$$

Their work presented theoretical maximum bubble diameters of $1.2mm$ (GLR=1%), $1.5mm$ (GLR=2%), and $3mm$ (GLR=4%). However, the experimental values of this parameter were significantly lower, being the closest $0.9mm$ at GLR of 1% and decreasing further as they increased GLR.

The spray droplet size (quantified using SMD) in effervescent atomizer is affected by a group of variables, which mainly consist of: liquid proprieties (ρ_L – liquid density, μ_l – liquid dynamic viscosity, and σ – surface tension), gas and liquid mass flow rates ($\dot{m}_g$ and $\dot{m}_l$), injection and ambient pressure (p_{inj} and p_{amb}), gas phase molecular weight (MW_g), atomizer exit orifice (D_e), the internal flow regime (bubbly, slug or annular), mixing chamber size and shape as well as the dimensions of the gas injection orifice. It is important to note that many of the variables that affect the spray droplet size also affect the bubble size. In the case of bubble size (D_b) it also depends on: $\dot{m}_g$ and $\dot{m}_l$, liquid proprieties, MW_g, among others such as coalescence additives.

This proves that bubble size has a strong influence over the spray droplet produced.

There are few mentions of correlations between the SMD and the bubble diameter. Rahman et al. [2012] was one of them, which proposed a correlation between these variables as well as its validation with the literature.

1.2.4. Operational and Performance Parameters: Effervescent Atomization

The representative operational and performance parameters in effervescent atomization based on typical values found in Shepard [2011] work, among others, and an adjustment on bubble typical size, as well as liquid maximum flow rate from Loebker and Empie Jr [1997], is given in Table 1.2. This shows the range of values for the main operational parameters of effervescent atomization and the performance parameters, such as droplet size. (The values are merely representative)

Droplet Size [μm]	Bubble Size [mm]	Maximum Liquid Flux [kg/h]	Exit Diameter [mm]	GLR [%]
5 - 340	0.1 - 2.57	1800	0.1 - 2.5	0.01 - 4

Table 1.2: Operational and performance parameters in effervescent atomization. Values extracted from [Loebker and Empie Jr, 1997, Rahman et al., 2012, Shepard, 2011, Sovani et al., 2001, Sun et al., 2019].

1.2.5. Boiling on Thin wires

To produce bubbles of a certain size, similar to those injected in effervescent atomizers, reviewing the literature and implementing experimental techniques used for boiling processes was necessary.

The experiment made by Nukiyama [1966] was an important breakthrough for the classical boiling theory. The experiment used a metallic wire (setup used in Fig. 1.6), where the temperature and heat flux were evaluated. Nukiyama's investigated the boiling of the heating wire under saturated liquid and obtained the boiling curves ($Q - \Delta T$ and $\alpha - \Delta T$). He created a simple electronic system that generated and controlled bubbles by supplying a certain amount of electric power to the wire.

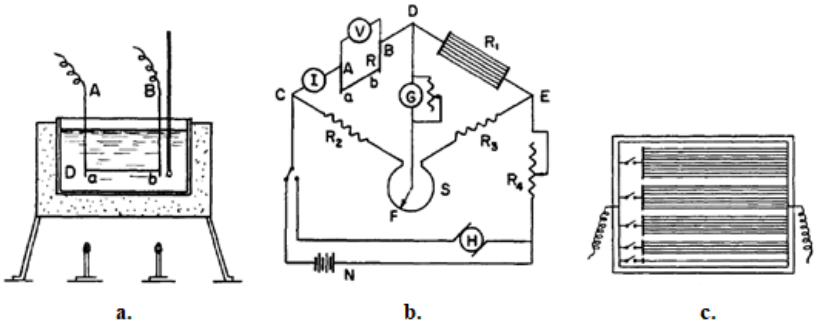

Figure 1.6: Experimental setup used by Nukiyama [1966] for metal wires.

This experiment used thin wires so that low electric power was required to reach high-heat fluxes.

Boiling occurs in the interface solid-liquid when a liquid comes in contact with a heated surface that is sufficiently higher than the saturated temperature (T_{sat}) of the liquid. For water: $T_{sat} \approx 100°C$ at $p = 1atm$.

In pool boiling, without liquid flow, the liquid movement is due to the natural convection currents and provokes bubble movement under the influence of impulsion forces. Subcooled boiling (or local nucleate boiling) is when the overall liquid temperature is below the saturated temperature. In Nucleate boiling, the liquid temperature equals T_{sat}.

In the single-phase convection regime, bubbles only start to form when the liquid in contact with the heating element increases at least $2°C$ to $6°C$, in water, above the T_{sat}. The liquid phase change, evaporation, occurs only in the solid-liquid interface.

The region AB includes the regime of isolated bubbles (where some bubbles collapse and condensate into the liquid), followed by the regime of jets and columns of vapor bubbles that flow to the free surface. The regions BC and CD represent the transition of the boiling phenomena to slug flow until it reaches a fully developed annular flow. In the regime of transition boiling, nucleate boiling and film boiling can be seen, although extremely hard, since a typical boiling process does not go along the curve, suddenly jumping from point B to point D, as seen in Fig. 1.7. Point B reaches the critical heat flow value ("burnout point"), which may exceed the heating element melting point. These regions are far more complex than the first stages of boiling.

Nowadays, several articles are studying the boiling process in pool boiling (subcooled and nucleate boiling), either using wires or plates in different configurations and orientations, as well as in normal gravity and microgravity. These articles include

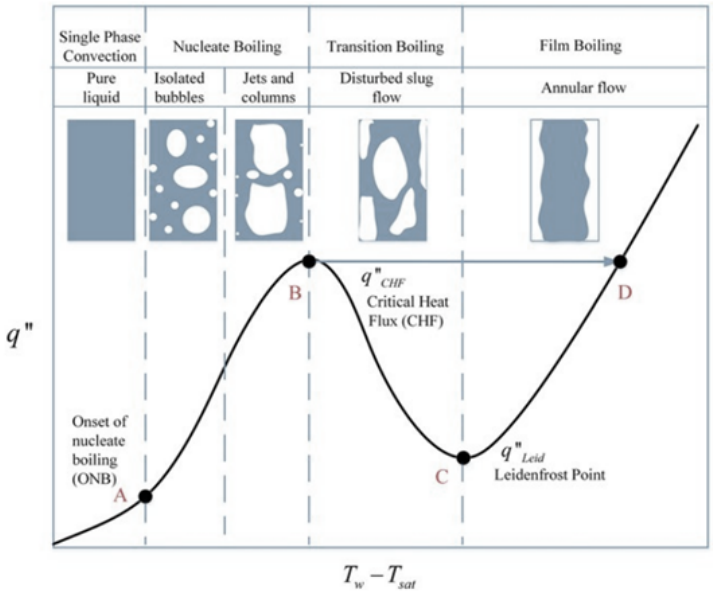

Figure 1.7: Typical Boiling curve [Hu et al., 2017].

bubble dynamics (Zhao et al. [2008]), bubble attachment and sweeping (Xu et al. [2021]), coalesced bubble detachment frequency (Kumada et al. [1995]), bubble explosion (Wang et al. [2016]), bubble oscillation (Lu and Peng [2008]), bubble slippage (Lu and Peng [2006]), bubble behavior variation with heat flux in the case of heating wires by changing its orientation (Pi and Rangwala [2019]), as well as bubble flow in subcooled boiling (Wang et al. [2005]) and bubble phenomenon's (such as micro-bubbles return phenomena in (Wang et al. [2007]). Understanding bubble behavior is crucial in boiling heat transfer. The characteristics of the pool boiling process are affected mainly by bubble dynamics.

The dynamic behaviors of vapor bubbles and the typical process of coalescence, vibration, and departure of bubbles in the regime of fully developed nucleate pool boiling with high heat flux was observed by Zhao et al. [2008]. The coalescence between adjacent bubbles was seen and the detachment of smaller bubbles occurred more frequently. It was found that the vibration due to the coalescence of adjacent bubbles is one of the reasons for bubble departure.

Observations done by Straub [2001] said that the bubble departure is attributed to surface tension effects, to "bubble ripening" and coalescence processes.

1.2.6. Subcooled Boiling on Thin wires

Nukiyama's experiment was done with saturated liquid, meaning that the liquid temperature was at T_{sat}. As mentioned before, in subcooled boiling, this is not the case.

Wang et al. [2005] investigated the bubble dynamics and interfacial transport phenomena in subcooled boiling on ultra-thin platinum wires ($0.025mm$ and $0.1mm$), similar to the work made by Marek and Straub [2001], which said that moderate heat fluxes are only transferable by natural and forced convection. Fig. 1.8 shows the experimental setup use by Wang et al. [2005].

Their work mostly focused on single bubbles and appears to have produced very

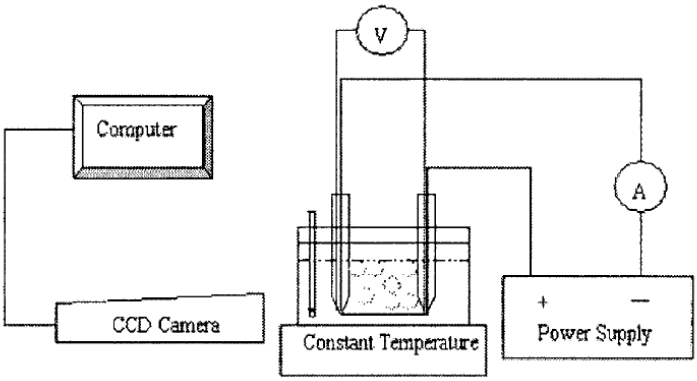

Figure 1.8: Experimental Setup used by Wang et al. [2005].

small bubble sizes, being one most mentioned of $D_b = 0.03mm$.

Xu et al. [2021] analyzed the bubble attachment and sweeping phenomena on micro-wires in subcooled pool boiling. One of the wires used by Xu and his colleagues experiment was $D_w = 150\mu m$ NiCr wires with $100mm$ in length. The experimental setup was similar to the aforementioned one. The analysis was made for different power supplies ranging from $25.4W$ to $45.5W$ for the NiCr wire. It was not presented a bubble size distribution since their main focus was to analyze the interaction phenomenons between bubbles and the heated wire, however, from the scaled images presented, one can have a rough idea of the bubble size produced. Bubbles showed to have diameters from $0.08mm$ to $0.57mm$ for smaller heat fluxes.

Kumada et al. [1995] measured the detachment frequency of coalesced bubbles from thin horizontal wires (0.1 to $3mm$). The experiment with wires included NiCr wires from 0.1 to $0.5mm$ in diameter and lengths between 80 to $180mm$. Fig. 1.9 shows the experimental setup used for their experiment. Some of the acquired data when water was used as the liquid at atmospheric pressure and room temperature displayed bubble sizes smaller than $1mm$.

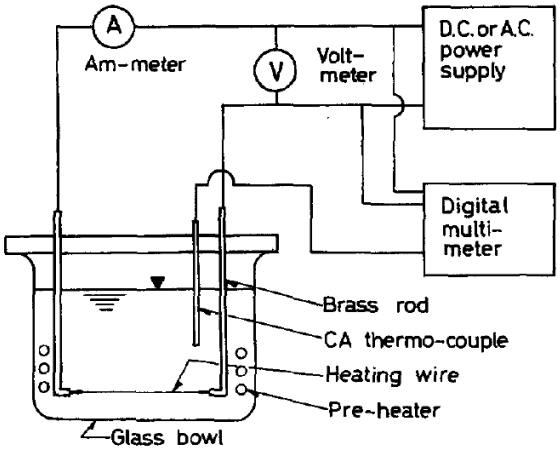

Figure 1.9: Experimental Setup used by Kumada et al. [1995].

In conclusion, there are many experiments made to study the subcooled boiling process in the available literature. However, each individual study is focused on a particular set of parameters and/or phenomenons. For this dissertation, the experi-

mental apparatus is more simplistic, and the main goal is to be able to observe bubbles characteristics in terms of power supply, primarily without pre-heating the liquid.

2. Experimental Setup: Bubble Generation

An experimental apparatus was built to evaluate the theory of inducing bubbles thermally inside an effervescent atomizer instead of introducing bubbles through mechanical work via the aerator section.

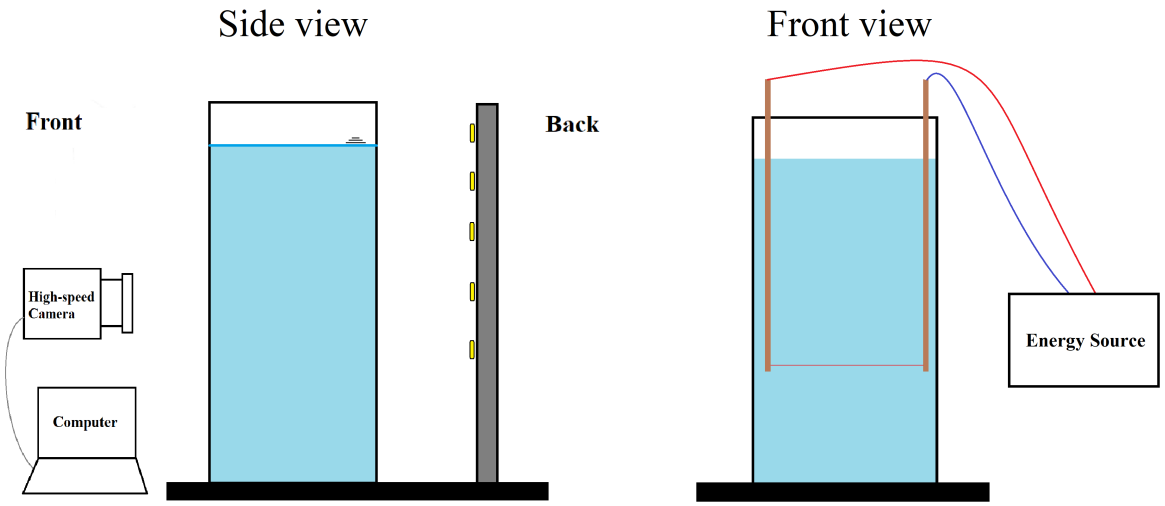

Figure 2.1: Simple setup illustration.

The experimental setup built is only the first of many steps to validate this possibility of a different effervescent atomization approach. This first step consists of the analyses of bubble behavior using a thin NiCr wire ($D_w = 100\mu m$ and lengths between $10mm$ and $12mm$), without fluid motion, in a vessel of similar dimensions to an actual atomizer. Distilled water was used as the liquid and the Vessel dimensions were ($20mm \times 20mm \times 100mm$). The structure design was made with the use of the software: Solidworks.

A couple of design variations were built due to unexpected issues encountered. The first design had dimensions of ($10mm \times 10mm \times 100mm$), and the connection between cooper and Nichrome wires was on the sides of the printed structure. However, this presented a couple of challenges. The holes on the sides had to be isolated so that there was no liquid leakage, and in case the wire 'burned out' the experiments had to be delayed. Another idea was to use a ceramic piece to connect the wires, however, it was never implemented. The latest design is similar to Nukiyama's experiment (among others) in terms of how the power is supplied to the testing wire, which was through the top of the vessel using copper wires as the connectors.

The tolerance given was $0.15mm$ between pieces for a proper fitting due to slight discrepancies in the printed structure components. In Fig. 2.2a is the base of the experimental apparatus. The base has small holes on each corner to be able to fix the installation in place, as well as a guiding 'rail' in the middle to allow the movement of

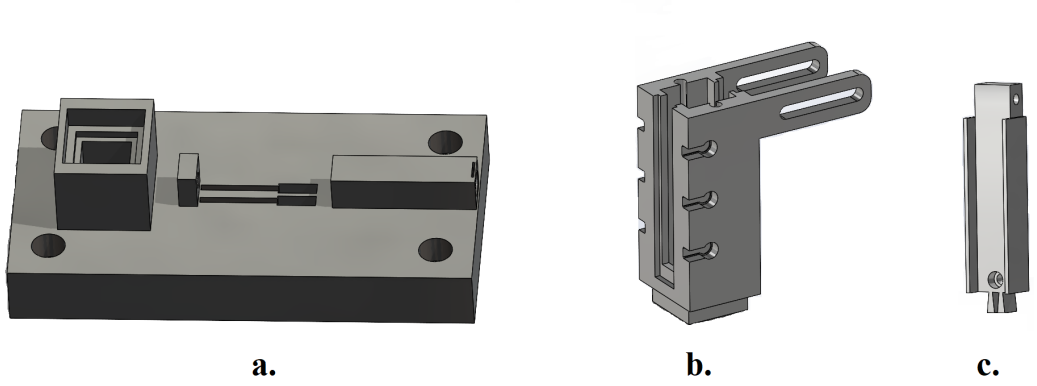

Figure 2.2: Solidworks separate pieces: a. Base ; b. Top Part ; c. LED's Support.

the LED's Support, Fig. 2.2c, in addition to a hole shown on the left side where the Fig. 2.2b would fit. The printed piece Fig. 2.2c intent was not only to tape LED's to be used as a light source but also to allow the adjustment of lightning viewed inside the vessel on the front side. This adjustment could be done with a helical screw to move the LED's closer or farther from the testing area.

The three holes on each side of the 'Top Part' were intended to secure piezoelectric sensors to measure the vibration produced in the local nucleate boiling process. The intention was to get an informational signature (based on the information theory) to get a correlation between vibrations and bubble morphology. However, the work at hand proved to be challenging as it is, meaning this plan was disregarded.

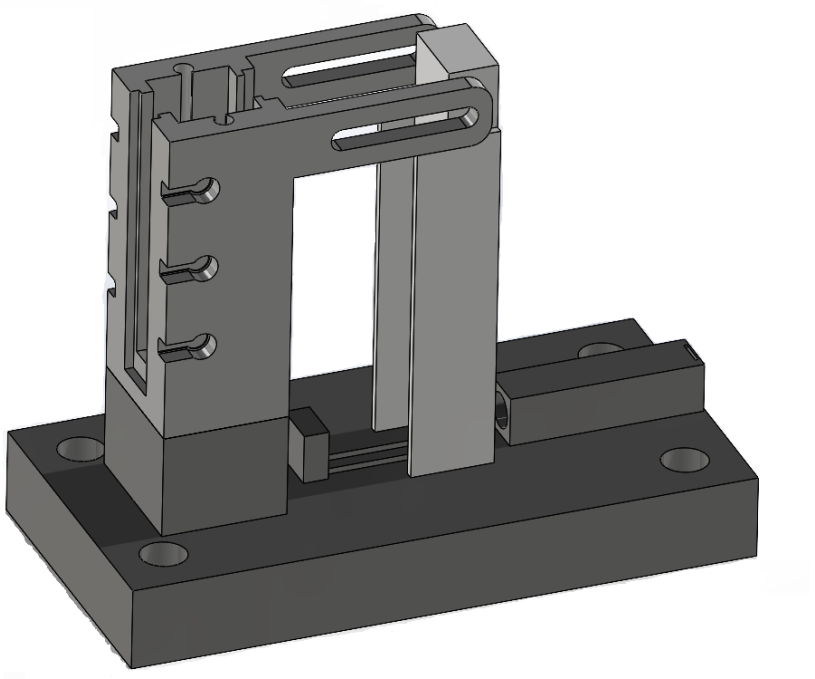

Figure 2.3: Solidworks - Final Experimental Setup design.

The experimental apparatus designs are detailed in Appendix A.

The apparatus structure was $3D$ printed using Prusa i3 MK3, and the material used was Polyethylene Terephthalate Glycol (PETG). Although PETG's transition temperature is around $85°C$, where the material starts to soften, the experiments made were about 100 seconds at maximum (with a few exceptions), which made it possible to run multiple experiments before the vessel was compromised. Also, the heated wire was ensured not to touch the printed material, and the maximum current supplied to the wire was $i = 3.1A$ ($q_w = 31.9W$).

Although the temperature has an effect on bubble behavior, temperature measurement was not the main focus. The temperature of the volume of liquid inside the vessel was considerably lower than the saturated temperature, only reaching higher temperatures on and around the heated wire.

Fig. 2.3 shows the experimental setup design used throughout the latest experiments. More than one of these was mounted and used. The setup has a transparent glass for visualizing the bubbly regime morphology induced by the first stages of boiling and an opaline glass to allow light to pass through. A few LEDs ($12V$) were used as the light source, which was taped to the movable printed piece shown in Fig. 2.2c. The Nichrome wire was connected to two larger Copper wires with about $2mm$ in diameter, which is twenty times larger than the testing wire. The purpose of this was only to carry the electrical current to heat up the testing wire without heating the larger copper wires. A supply source with a current maximum range of $i = 3.1A$ was used as the energy provider. And the energy source automatically measured the voltage applied, with an incorporated voltmeter and ammeter. The energy source was also used to supply power to the LEDs on the back of the setup. DC power is provided with a range of $8.6W$ to $31.9W$.

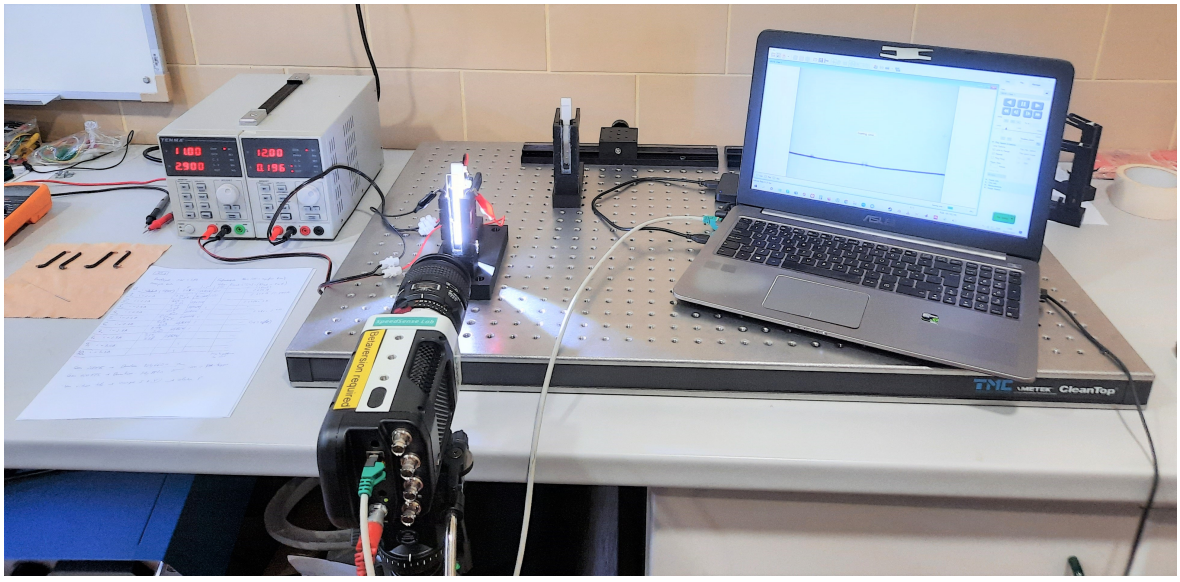

Figure 2.4: Experimental Workbench.

In this study, five different video sample rates were captured by the high-speed camera: 200 Frames per Second (FPS) with around $\Delta t = 84.6s$ (results not included in the Chapter 3, only in Appendix A); 600 FPS with $\Delta t = 28.2s$; 2000 FPS with $\Delta t = 8.7s$ (only in Appendix A); 12000 FPS with only $\Delta t = 1.67s$; and 51000 FPS with $2.16 - 2.45$ seconds. The image resolution was kept the same 512×384 for almost all experiments, except the 51000 FPS videos, which had a resolution of 256×128.

Moreover, the 51000 FPS videos were focused only on a single wire location. The higher frame rates' purpose was to view the beginning of bubble generation, as well as the collapse time of bubbles, and lower frame rates to view the first stages of the boiling phenomena in a slightly longer period.

The following Fig. 2.5 and Fig. 2.6 shows the main equipment utilized in the elaboration of this dissertation.

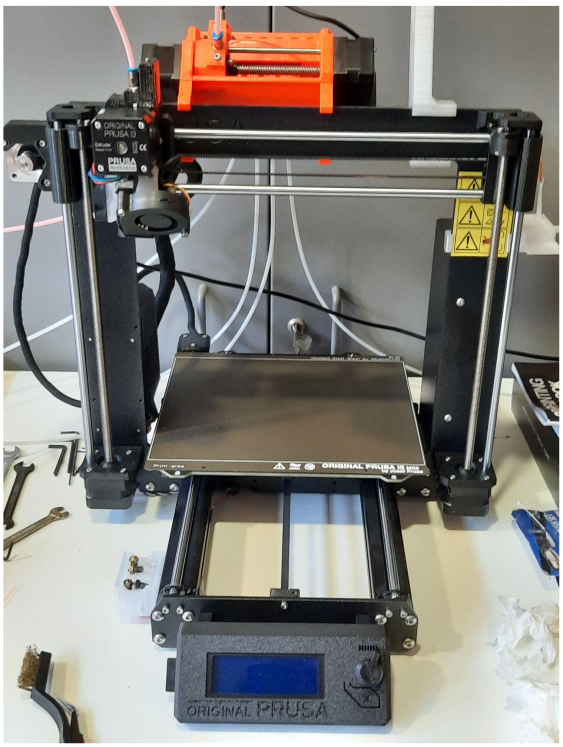

Figure 2.5: 3*D* printer - Original Prusa i3 MK3.

a. **b.**

Figure 2.6: a. DANTEC Dynamics: Phantom Miro M340; b. Power Source: Tenma 72-10505.

2.1. Experimental Considerations

The channel geometry is squared to position one or multiple wires with different orientations. In the current study, it was used only one horizontal wire. Nucleate boiling regime heat fluxes in water, vary between $q''_{min} = 10^2 kWm^{-2}$ and $q''_{max} = 10^4 kWm^{-2}$.

The power required to generate bubbles using a nichrome wire of $100\mu m$ with high resistivity ($\rho_R = 10^{-6}\Omega m$), and with a length around $L_w = 10mm$, would be between $q_{min} = 0.314W$ and $q_{max} = 31.4W$. Given the nichrome wires dimensions, it would need an electric current (i_w) between $0.497A$ and $4.967A$.

2.2. Experimental Procedure

To start each experiment the energy source was turned on for the current input desired. As soon as the current started to pass through the Nichrome wire, bubbles started to form slowly, picking up speed rapidly the higher the power supplied. The videos taken with the high-speed camera started roughly at the same time as the power source was turned on. The camera had a pre-trigger timer in order not to miss the initial local boiling process. This was useful so that the camera could capture the moment before local boiling started to occur which allowed us to get a reference background image for each test, which was useful later on in the image processing analysis. The voltage measurements were displayed in the energy source and registered manually. The input power was then calculated with the formula of Ohm's law.

Each experiment started with a current equal to $1.7A$ which was gradually increased by $0.1A$ for the following test, until it reached the maximum current of $3.1A$

The initial boiling phenomena were observed, captured, and stored in a computer for further analysis.

2.3. Experimental Diagnostic Techniques

Varying the supplied power, the goal was to analyze the bubble size distribution (BSD) and bubble formation rate for the bubbles that remained in the liquid after detaching from the wire, and the time since formation until departure, was to make a relation between power supplied and formed bubbles characteristics.

However, the time spent by the liquid inside the vessel was supposed to be extremely short since its purpose application is for atomization. And in an atomization process, the liquid that goes through the atomizer remains inside for a short period of time. On that note, it was also taken into consideration the bubbles formed that remained attached to the wire, their size and growth velocity was determined for a defined interval.

All observed phenomena were recorded by the high-speed camera Phantom Miro M340, which has up to 3.2 Gigapixels-per-second (Gpx/s) with 800FPS at a full resolution of 2560×1600. To facilitate the measurements of these parameters in 15 thousand-plus images in these experiments, this task needed to be automated. An image processing algorithm, using the software Matlab, was developed to determine the bubble characteristics and behavior.

Firstly, a visual bubble count was done for each test to evaluate the necessity of having to use an algorithm. Most of the experiments made, especially with a lower

power supply, produced an extremely low count of bubbles. These tests were deemed redundant and initially, only a visual analysis was made.

For the bubble measurement techniques, a simple Matlab function was used as the base code to detect bubbles within the frames. The function "ImFindCircles" proved to detect reasonably well larger bubbles, however, smaller bubbles were not detected accurately in many cases.

In Fig. 2.7 a and b, one can see the original frame and circles (bubbles) identified by this function. In the second image, the arrows point to bubbles that were detected but do not exist, these can be considered as 'phantom bubbles'. To solve this issue a variety of alterations to the original image were made in order to increase accuracy. The background is mostly bright, with the exception of the wire. Fig. 2.7c is the product of removing the image from the background with an increase in pixel value +100 as well as a contrast enhancement.

This presented better results, which removed most of those 'phantom bubbles' mentioned.

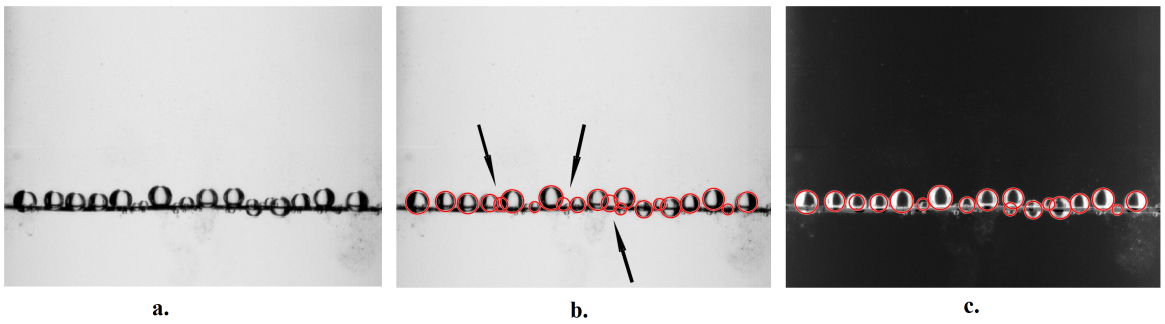

Figure 2.7: Bubbles detected by the algorithm, Matlab function 'ImFindCircles': a. Original frame; b. Bubble detection with original frame; c. Bubble detection with altered frame.

The image resolution was determined by analyzing each column variation of pixel values in the background image, where the wire presents low values corresponding to the color black or close to it. Knowing the wire's diameter ($D_w = 100\mu m$), it can be used as the reference object to obtain the dimension of each pixel for the different experiments. The image resolution error with this method was remarkably low, which is about 0.5%.

The image resolution results for the value of 1 pixel vary between $15\mu m$ and $20\mu m$ for all the experiments made. For test with $\Delta t = 1.67s$, 1 $pixel \approx 16\mu m$

One of the main concerns with the function shown in Fig. 2.7 is the imprecision in identifying small bubbles. The 'ImFindcircles' function only detects bubbles, with good accuracy, above 5 pixels. Thus, the algorithm had to take into account the previous two frames and the following of the one being analysed so that detections that occur in one of those that do not match the others are discarded. The issues concerning overlapping bubbles and/or the detection of bubbles within other bubbles also needed to be addressed and eliminated.

Furthermore, the algorithm developed enables the possibility of analysing bubble size with the information theory, and isolates growing bubbles which produces bubble data which was critical in the outcome of the results obtained in Chapter 3. This data consists of time, bubble size, growth rate, and positioning within the frame.

Finally, it has the ability utilizing the data acquire to generate a non-linear curve

of the bubble growth evolution through the equation $D_b = at^b$, where a and b are the scale and shape parameters, respectively, which bests portrait bubble expansion.

3. Results and Discussion

The purpose of these experiments was to study bubble morphology and behavior in local nucleate boiling and evaluate the possibility of forming bubbles within a timescale compatible with their dragging when subjected to a flowing liquid.

3.1. Bubble formation and interaction phenomenology

The multiple bubbles observed with an electric power range between $8.6 - 31.9W$ are similar to those found in the literature, as were several of the bubble dynamical phenomena observed. For example, bubble slippage occurs more frequently at a liquid temperature of around 40°C and heat fluxes in the range of $40 - 80W/cm^2$ according to Lu and Peng [2006], without preheating, it is a rare phenomenon but observable, nonetheless, as depicted in Fig. 3.1 where the bubble movement from left to right along the surface of the heated wire is clear.

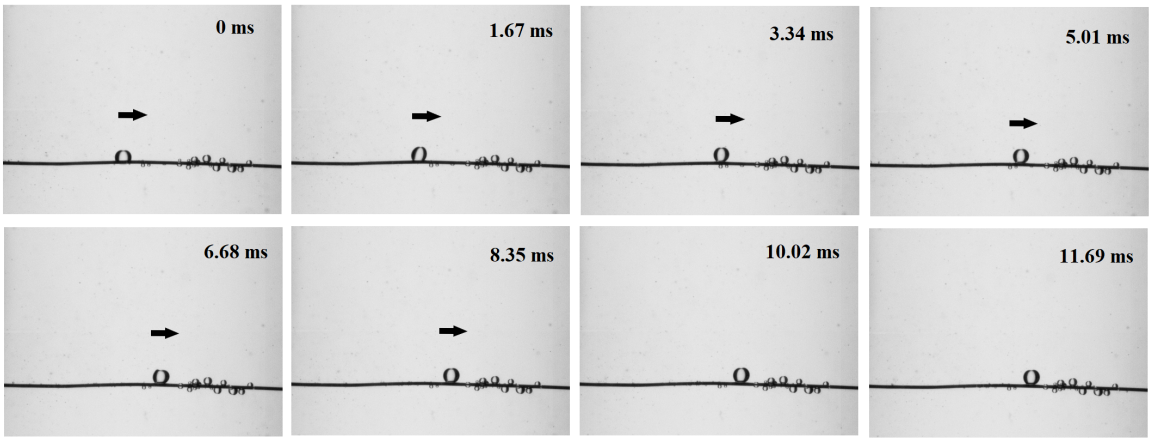

Figure 3.1: Bubble slippage example.

A more common and frequent behavior observed was the merging of adjacent bubbles. In some cases, this merging led to bubble sizes that departed from the wire when buoyancy forces overcame the surface tension ones. Fig. 3.2 exemplifies the bubbles merging and detaching after $23.38ms$. Also, bubble departures often occur after the collapse of adjacent bubbles.

Bubble leap is clearly seen in Fig. 3.3, where the bubble returns to the wire after detachment. This is likely due to the Marangoni force, which tends to attract bubbles to a heated surface due to temperature differences. One can also see the departure of three separate bubbles in this image.

During the experiments, an interesting interaction occurred between two large bubbles and two smaller ones (Fig. 3.4), with the smaller ones hovering between the large ones. This event lasted around $2.01s$, after which departure occurred. Also, $0.4s$ after

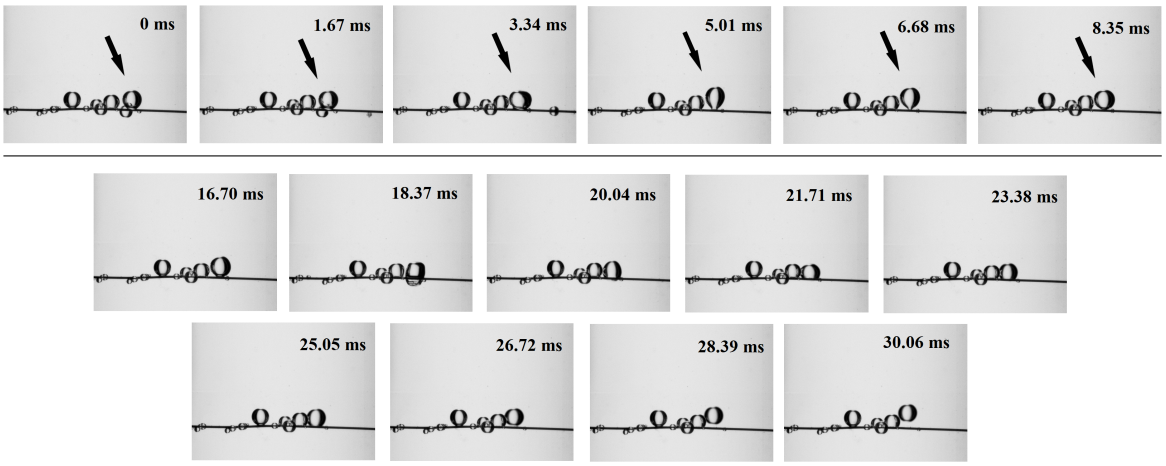

Figure 3.2: Bubble merge and departure from wire.

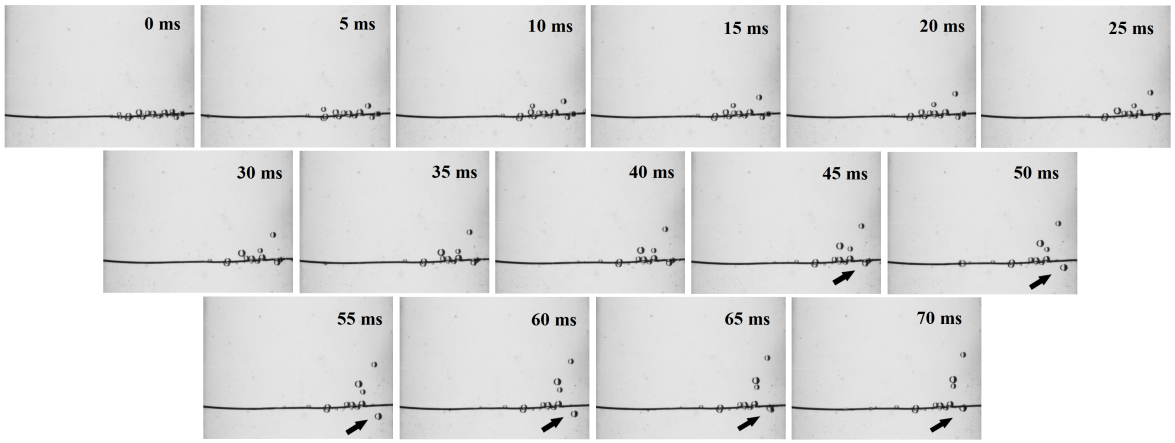

Figure 3.3: Bubble leap on heated wire and three bubbles departure.

the hovering started, the small bubbles merged and kept interacting with the large ones.

In Fig. 3.4, one can also see the collapse of bubbles affects the ones on the wire (where the bubbles appear distorted), which usually promotes departure. Another event, similar to the one observed by Xu et al. [2021], was the circling of very small bubbles around larger ones, in these cases, not easily identified because of the images lower resolution relative to their size (close to a pixel), but discernible by their movement.

After identifying several of the observed phenomena, the applicability of thermally induced bubble generation to effervescent atomization depends on the corresponding frequency. In Appendix A is shown the bubble generation frequency in terms of bubbles number in a certain Δt.

3.2. Phenomenology of bubble formation and growth

To implement a bubble generation strategy through local nucleate boiling in effervescent atomization, one needs compatibility between bubble growth time and the liquid flow time scale inside the atomizer. In the initial stages of boiling, most of the bubbles remain attached to the wire, with a few exceptions. For higher input power

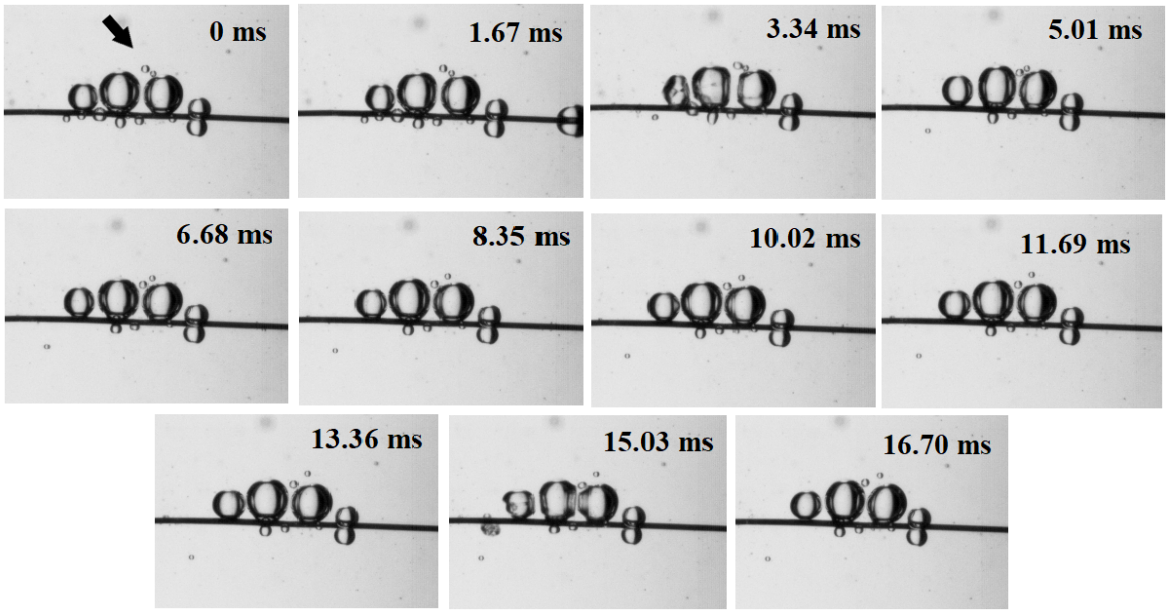

Figure 3.4: Two small bubbles interacting with two bigger bubbles.

supplies, smaller bubbles release and remain suspended in the liquid. With a liquid flow, the bubbles would likely be convected and contribute to the effervescent effect at the nozzle exit.

For the image processing analysis, an algorithm was developed in Matlab to determine the number of bubbles formed, the corresponding diameter (D_b) and Bubble Growth Velocity (BGV) for a specific range of supplied power. The first set of tests considered a time interval of $\Delta t = 1.67s$, while a second set enlarged the acquisition time to $\Delta t = 28.2s$. The maximum bubble diameter detected ($D_{b,max}$) in the first test was $560.52\mu m$ for power input of $28.551W$. In the second set of tests, the experiments with a current equal to or larger than $2.2A$ begin showing voltage variability, indicating a possible change in the resistivity of the wire. Although investigating this event further is beyond the scope of the present dissertation, it could represent a limitation of the bubble generation strategy worth considering in future work. When processing images, a few bubbles have significantly short lifetimes, corresponding to intense growth and collapse. These bubbles were sorted and not considered in the bubble growth analysis. The advantage of the second set of tests is to assess whether or not bubbles grow to a size where buoyancy forces lead to their detachment from the wire. Fig. 3.5 shows the bubbles' median diameter as a function of the dissipated heat transfer rate. The results evidence how the size in the first $2s$ after bubbles begin forming is independent of the heat transfer rate. At the same time, a larger acquisition time allows bubbles to grow, increasing their median diameter. With $\Delta t = 28.2s$, for $q_w > 17.5$W, no data exists because bubbles form and collapse almost instantaneously.

The maximum number of bubbles obtained in each frame (representing a given instant) was higher for longer tests. However, when their departure implied a short duration between formation, detachment, and collapse, measuring their size and growth velocity was difficult and not as crucial as those remaining attached to the wire. Fig. 3.6 shows two examples for the first and second set of tests.

Moreover, several bubbles identified in the image processing algorithm have a momentary presence, and the bubble validation criteria demand the presence of a bubble

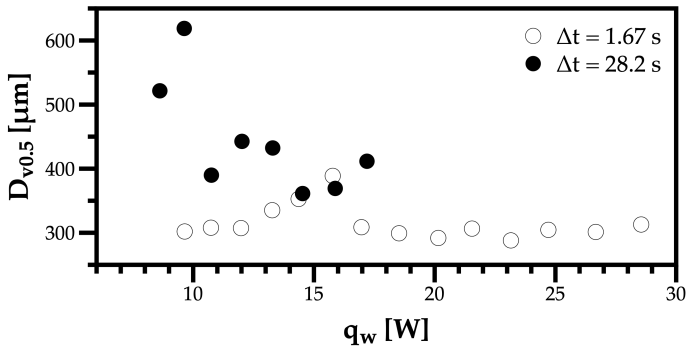

Figure 3.5: Bubble size representing 50% of bubbles volume (median diameter, $D_{v0.5}$ $[\mu m]$) as a function of dissipated heat transfer rate (q_w $[W]$).

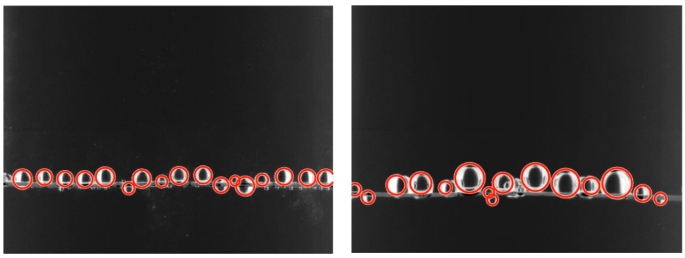

Figure 3.6: Example Of quantifying the number of bubbles in each frame: a. Tests 1 - $q_w = 28.551W$ (after $t = 1.48s$); b. Tests 2 - $q_w = 8.619W$ (after $t = 21.59s$).

in frame t_i, also in frames t_{i-2}, t_{i-1}, and t_{i+1}. Therefore, the maximum number of simultaneous bubbles obtained for each power input is depicted in Fig. 3.8. For the set of tests with $\Delta t = 28.2s$, the values do not include bubbles formed for $q_w > 17$W because the time attached to the wire was less than $4/f_{aq}$, which is $f_{aq} = 600$ FPS in the second set, equivalent to $6.7ms$ between t_{i-2} and t_{i+1} relatively to the frame under consideration at t_i. For example, Fig. 3.7 shows the formation and collapse of a bubble with a power supply of $14W$. The image acquisition rate in this test was 51000 FPS to observe and quantify the time for this phenomenon. The bubble reaches its full size after $78.4\mu s$, after which begins to shrink until collapses.

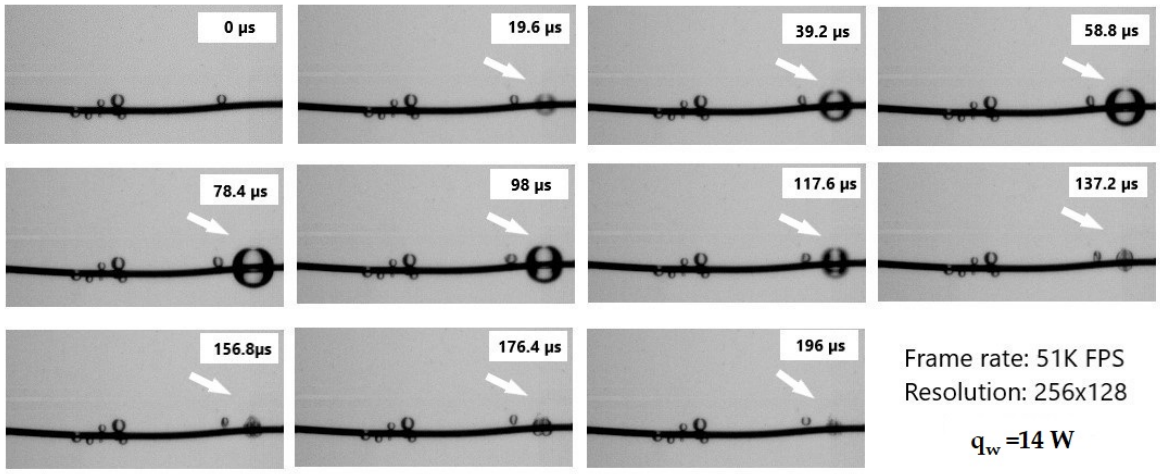

Figure 3.7: Time of a bubble formation and collapse at $q_w = 14W$.

For the smaller Δt conditions (Fig. 3.8a.), there is no clear evidence for the relation between the maximum number of bubbles and the power input, while in the second case (Fig. 3.8b.), for $q_w > 12$W, this number decreases for the aforementioned reasons of smaller time intervals attached to the wire.

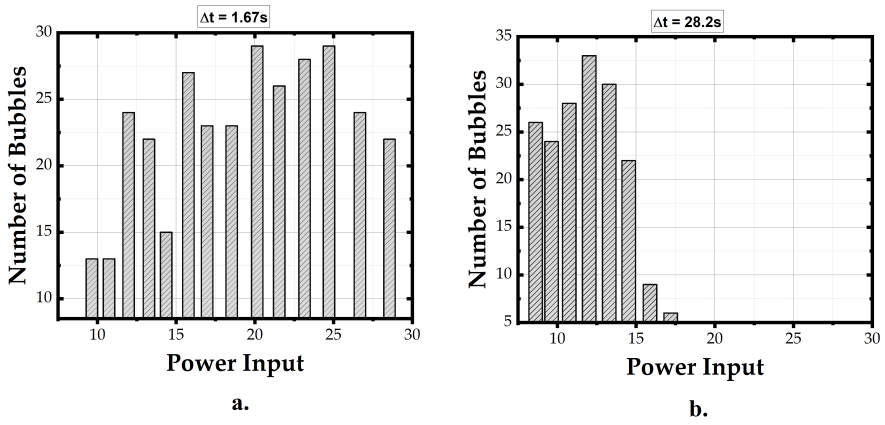

Figure 3.8: Maximum number of bubbles in a single frame: a. $\Delta t = 1.67s$; b. $\Delta t = 28.2s$.

Another reason that may have affected the number of bubbles and their size for higher power input was most likely the wire vibration. For example, the tests with 31.946W have shown a violent wire oscillation contributing to bubbles detachment without growing to the sizes reported later in the cumulative frequency distributions.

The statistical analysis in the algorithm considers a temporal accumulation of bubble sizes measured in each frame. Therefore, a bubble size measured in a certain position, whether changing its size or not, may represent multiple counts in the final sample. Therefore, after dividing by classes, the number of bubbles in each class k, n_k, expresses a not only counts but *temporal presence* in the sample. For this reason, the results presented consider the cumulative number-weighted bubble size distributions for different power inputs.

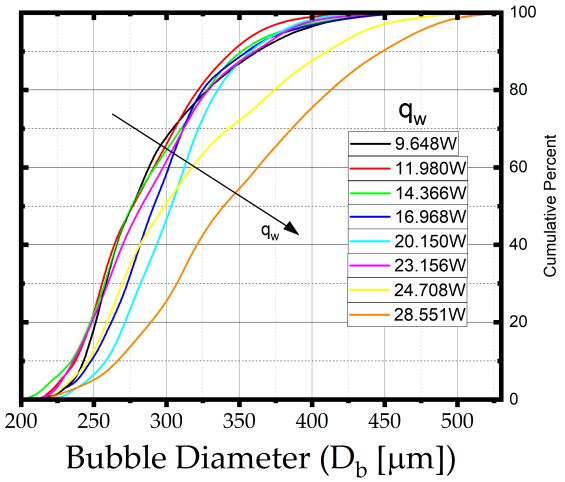

Figure 3.9: Bubble size cumulative distribution - Set of tests 1 ($\Delta t = 1.67s$).

A sharper rising of the cumulative frequency means closeness to a uniform distribution of bubbles with similar sizes around the median. For power supplies between $9.648W$ and $23.156W$, the curves are somewhat similar. Fig. 3.9 shows a gradual decrease of the cumulative frequency slope with larger input power values, implying a larger polydispersion of bubble sizes. Following the terminology of [Panão et al., 2020] adapted to Bubble Size Diversity (BSDy), the normalized Shannon entropy (H_n) assesses the polydispersion degree (how many different sizes are relevant in the bubbly flow). The volume-weighted Standard Deviation (SD_v) assesses the heterogeneity degree (how different are the relevant sizes in the bubble flow). Fig. 3.10 shows that longer formation and growing time intervals tend to produce a larger diversity of sizes of bubbles formed on the wire.

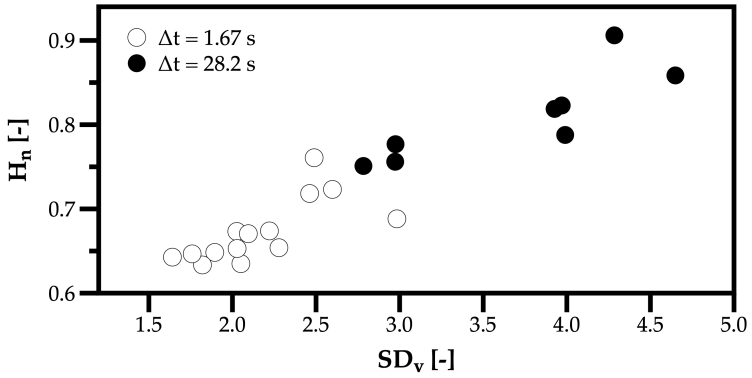

Figure 3.10: Bubble Size Diversity assessed through the polydispersion (H_n) and heterogeneity (SD_v) degrees for the shorter ($\Delta t = 1.67s$) and longer ($\Delta t = 28.2s$) sets of tests.

This result leads to the final analysis dedicated to bubble growth. Characterizing bubble growth dynamics (size and velocity) is not straightforward because bubbles do not form at identical times or locations. Therefore, any analysis is restricted to short intervals, without covering all the length from bubble formation until departure. Fig. 3.11 exemplifies two cases related to bubble growth dynamics. The first shows the evolution of a single bubble with departure followed by another bubble formation and consequent release (Fig. 3.11a.), and the second shows the merging of two bubbles (Fig. 3.11b.).

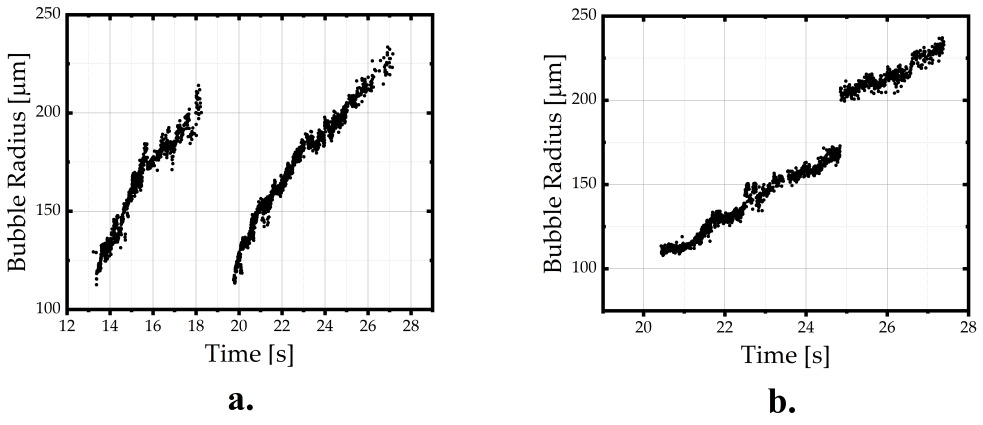

Figure 3.11: Examples of data acquired to determine BGV [$\mu m/s$] at $q_w = 10.754W$, Tests 2 ($\Delta t = 28.2s$): a. The growth of two bubbles and their departure; b. Influence of merging bubbles on size.

In Fig. 3.12, although the initial bubble size does not match between these three examples, one can easily see that the bubble growth velocity for $q_w = 10.754W$ is slightly higher than the other two. However, to assess the effect of the power input, one uses a non-linear curve fitting.

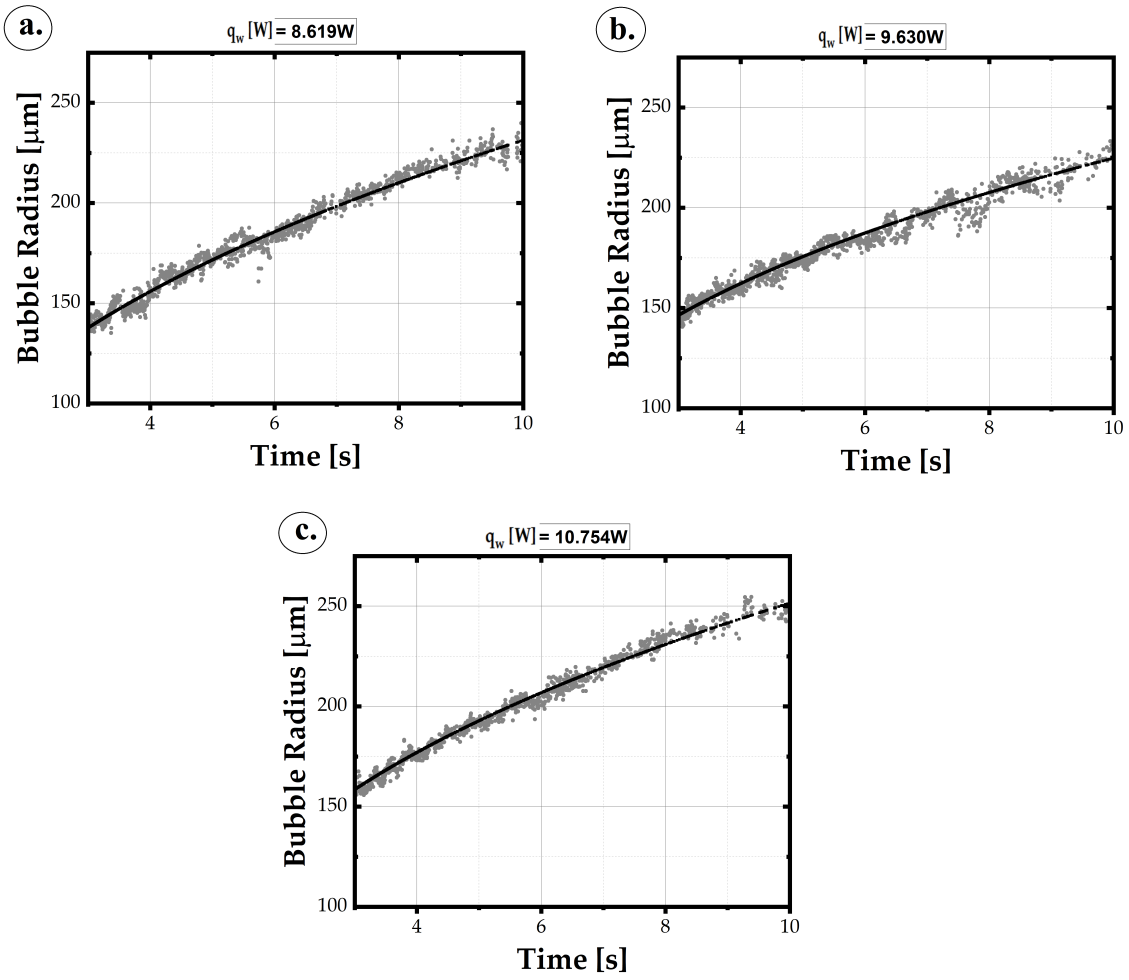

Figure 3.12: Three examples of Bubble Growth for three different power input in the same timescale: a. $q_w = 8.619W$; b. $q_w = 9.630W$; c. $q_w = 10.754W$.

The equation that best described bubble size growth is non-linear and expressed as $D_b = at^b$. The coefficients a and b are the scale and shape parameters, respectively. Evaluating the effect of increasing the input power on the bubble growth rate means considering $dD_b/dt = a \cdot bt^{b-1}$. Since $b < 1$, bubble growth tends to stabilize with time. However, an analysis on the scale $a \cdot b$ might provide some insight into the effect of the input power. Fig. 3.13 depicts this result and emphasizes a faster bubble growth with an increased dissipated heat transfer rate.

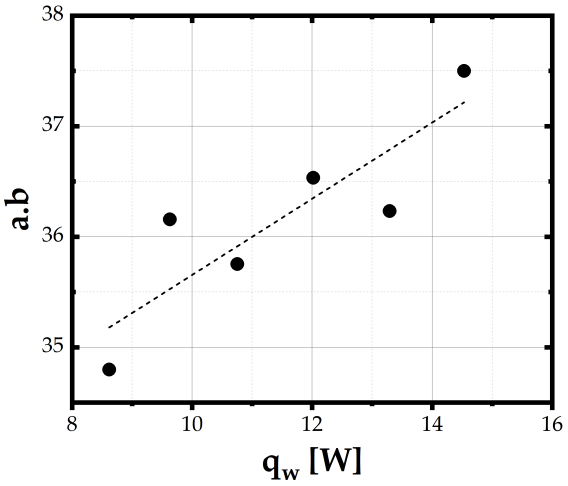

Figure 3.13: Coefficients a and b variation with dissipated heat transfer rate ($q_w[W]$). [Equation $D_b = at^b$]

4. Applicability of bubble formation and growth

A simple force balance analysis compares the force required to attach a bubble on the wire with the drag force exerted by a liquid flow. The usefulness of this analysis is to test the applicability of nucleate boiling to add gas to effervescent atomizers. The analysis begins with general considerations about the forces acting on bubbles in effervescent atomization.

4.1. Forces acting on bubbles in Effervescent Atomization

The individual forces acting on a single bubble transported by a liquid flow in effervescent atomization include surface tension (F_S), buoyancy (F_B), gas momentum flux (F_M), bubble inertial (F_I), and liquid drag (F_D). The combination of these forces determines the bubble size and was synthesized by Kim et al. [1994] as a common aeriated system using work to add gas bubbles as:

$$F_S = \sigma \pi d_{inj} f_n(\phi) \tag{4.1}$$

with σ as the liquid surface tension, d_{inj} the entry diameter injecting gas, and these authors define $f_n(\phi)$ as a term that considers the angle formed between the bubble center and the injection hole as the bubble grows.

$$F_B = \frac{\pi}{6} D_b^3 \left(\rho_L - \rho_G\right) g \tag{4.2}$$

with D_b as the bubble diameter, ρ_l, ρ_g the liquid and gas densities, respectively, and g as the gravitational acceleration.

$$F_M = \rho_G \frac{4\dot{V}_G^2}{\pi d_{inj}^2} \tag{4.3}$$

with $\dot{V}_g$ as the injected gas volume flow rate.

$$F_I = \frac{d}{dt}\left(m_b \frac{ds}{dt}\right) \tag{4.4}$$

with $m_b(ds/dt)$ as the momentum induced by the liquid motion surrounding the bubble. Finally, the drag force

$$F_D = \frac{1}{2} c_D \rho_L U_{eff}^2 A_{eff} \tag{4.5}$$

takes into account c_D as the drag coefficient, U_{eff} is the effective relative velocity and A_{eff} is the effective projected bubble area. The following section synthesizes the forces acting on the bubble produced in a thin hot wire.

4.2. Forces acting on bubbles in Subcooled Boiling

The forces acting on bubbles formed by local nucleate boiling events occurring on heated wires are the inertia and buoyancy forces (which provoke detachment from the wire) and the opposing surface tension force. Fig. 4.1 illustrates the several forces acting in bubble generation on a thin hot wire.

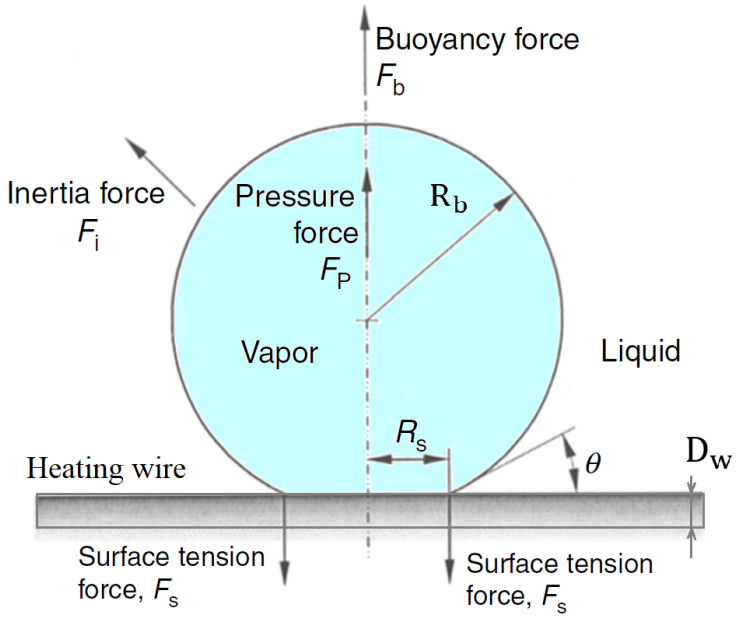

Figure 4.1: Forces acting on bubbles on a heated wire [Adapted from Ghazivini et al. [2022]].

In this case, the surface tension force differs from the formulation used in the case of injecting bubbles into the fluid flow, which depends on gas injection hole geometry, a strategy used to create the effervescent effect of a two-phase mixture that facility liquid atomization at the nozzle exit. The surface tension force is a capillary force that maintains the bubbles attached to the wire.

$$F_S = \sigma_L l \tag{4.6}$$

where l is the length perimeter of the bubble in contact with the wire. The surface tension force when bubbles form on the wire opposes the forces promoting its release. Namely, the Marangoni force results from the effect of temperature on surface tension, leading to the existence of a surface stress imbalance when the liquid interface is subjected to temperature variations.

$$F_M = 2K\pi \left|\sigma_T\right| T' R^2 \tag{4.7}$$

where σ_T is the temperature coefficient of surface tension, and T' is the temperature gradient. K is an empirical coefficient, experimentally determined, to modify the departure from the linear theory of Young et al. [1959]. However, for this analysis, Marangoni forces will not be considered. Finally, a simplified force balance analysis aims at providing an indication of the limitations of using local nucleate boiling in a hot thin wire to produce bubbles with appropriate characteristics for generating effervescent atomization.

4.3. Force balance Analysis

In the condition of liquid flowing through a channel (atomizer section before the nozzle), one can neglect buoyancy and inertia forces and consider, in this analysis, the surface tension and drag forces as the main ones acting on bubbles formed in the hot thin wire. Fig. 4.2 shows the variation of the drag coefficient obtained by Kumada et al. [1995] for several fluids, including water, showing that above a Reynolds number of $\mathrm{Re}_{D_h} > 10^3$, the drag coefficient is inversely proportional to this dimensionless number, $c_D \propto \mathrm{Re}_{D_h}^{-1}$, maintaining the correlation re-derived by Kang and Leal [1988] for these high Reynolds values as,

$$c_D = 48/\mathrm{Re}_{D_h} \tag{4.8}$$

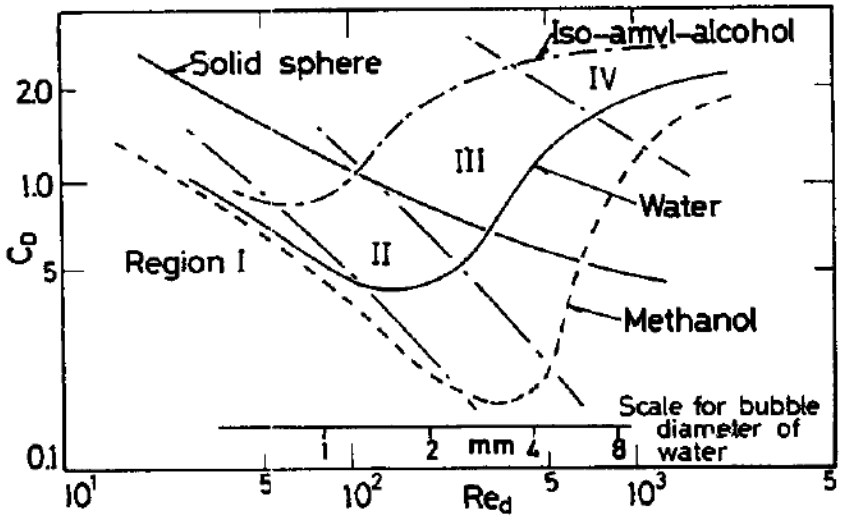

Figure 4.2: Drag coefficient and bubble Reynolds Number [Kumada et al. [1995]].

Surface tension forces keep the bubble attached to the wire, while drag forces will induce its detachment. Drag forces are proportional to the liquid flow velocity and limit the bubble growth observed in the previous chapter with a stagnated liquid pool. Therefore, drag forces tend to anticipate bubble detachment leading to the presence of smaller bubbles with a narrower size distribution. For bubble sizes with magnitude $D_b \sim \mathcal{O}(10^2)\ \mu m$, a simple scalar analysis shows a magnitude for drag forces for a velocity scale of $U_{eff} \sim \mathcal{O}(1)\ m/s$, $F_D \sim \mathcal{O}(10^{-7})\ N$, implying that once bubbles attached by surface tension forces reach a length scale of $l \sim \mathcal{O}(10)\ \mu m$, the liquid flow should drag these bubbles. The criterion for bubble detachment implies the drag force overcoming of the surface tension one,

$$F_S \leq F_D \tag{4.9}$$

which using Eqs. (4.5) and (4.6), including Eq. (4.8) for the c_D and considering the effective area as $A_{eff} = \frac{\pi}{4} D_b^2$, after some mathematical manipulation, the criterion reduces to

$$\phi \leq 6\pi \mathrm{Ca} \tag{4.10}$$

with $\phi = \frac{l}{D_b}$ and Ca as the Capillary number, $Ca = We/Re = \frac{\mu U_{eff}}{\sigma}$ that relates viscous drag forces with the surface tension ones. Assuming a minimum liquid flow

rate between $5.4kg/h$ (used by Sun et al. [2019]) and a maximum of $1800kg/h$ (see section 1.2.4), with a square cross-section duct area of $A = 1cm^2$ corresponding to the 10 μm thin wire used in the present experimental setup, the liquid velocity would be in the range $U_{eff} = 0.015 - 5$ [m/s]. For a water surface tension is $\sigma_L = 72.8mN/m$, and dynamic viscosity of $\mu_L = 8.9 \times 10^{-4} Pa \cdot s$ at an ambient temperature of 20°C, the Capillary number varies between 1.834×10^{-4} and 6.113×10^{-2}. Fig. 4.3 plots the criterion defined in Eq. (4.10).

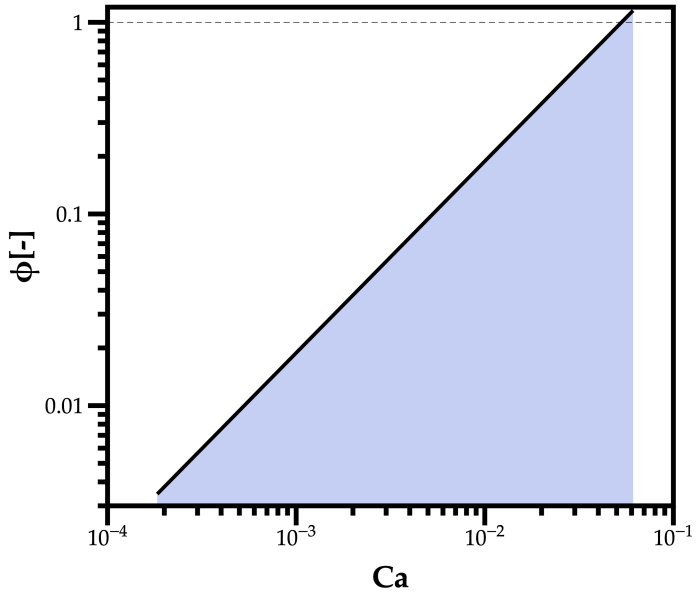

Figure 4.3: Relation of parameter ϕ and its variation with the Capillary number.

The value of $\phi = 1$ means the bubble contact length in the wire is equivalent to its size ($l = D_b$). The hypothesis of generating bubbles directly inside the atomizer works if there is enough time for bubbles to grow. It is reasonable to think that smaller bubbles at an early growth stage will likely fulfill the criterion. Therefore, this preliminary analysis suggests creating a low-velocity region around the wire to allow bubbles to grow, eventually using a bluff body upstream of the wire in relation to the flow direction. Fig. 4.4 illustrates this proposal.

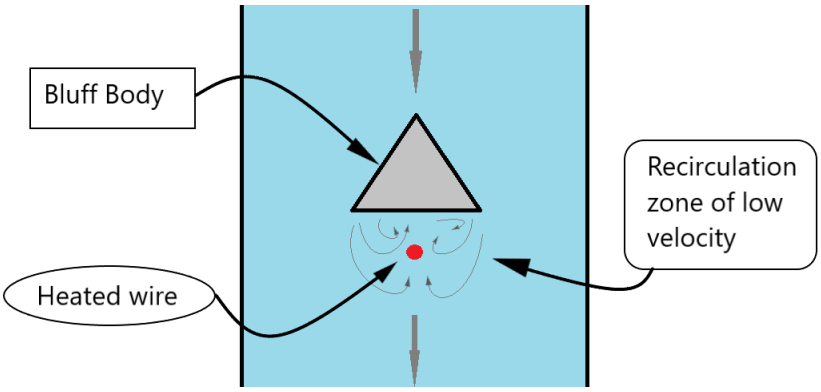

Figure 4.4: Bluff body illustration.

There are two advantages to this approach. Firstly, with a bluff body, the flow velocity field in the recirculation regions approaches the power input required to pro-

duce bubbles to the values used in this work because a liquid flow adds convective heat transfer losses when interacting with the wire. And secondly, with lower velocities, the capillary number will decrease, allowing the formation and growth of bubbles of considerable size ($\phi \leq 0.1$), favorable to the effervescent effect in the atomization process.

It is also noteworthy considering the time since bubble formation before collapsing contrasted to the time scale of liquid flow before reaching the nozzle exit and contributing to the atomization. It is possible that a few bubbles when subjected to the external force exerted by the flowing liquid, may not collapse and instead be dragged by the liquid flow. However, bubbles in this condition might have a diameter considerably smaller than the diameter reached before being detached from the wire and dragged by the liquid flow.

Considering the duct's length, $l = 100mm$, and using the same velocity range mentioned before, the traveling time, assuming Stokes flow around the bubble, would be: $[20; 6670]\ ms$. According to Nguyen et al. [2016], for a typical condensation rate of 10 mm/s, the collapse time is much larger than the traveling time, favoring the presence of generated bubbles at the nozzle exit.

5. Conclusion

The development of an effervescent atomizer with the hypothesis of using an electronically controlled bubble generation system which might reduce the input energy required to produce a spray has taken its first steps. A variety of bubble dynamical phenomena was observed of the same kind found in the literature. Some of them included bubble leap, slippage, and the merge of bubbles which occurred frequently.

A tendency of dissipated heat transfer rate with the coefficients which enables the ability to predict bubble size over time, to a certain degree, was determined. Moreover, the result shows evidence of how the size after $2s$ after bubble formation is independent of the heat transfer rate.

The generation of departed bubbles achieved was significantly low as well as their size when compared to effervescent atomization in the initial local nucleate boiling process, although in range, for power supplies $8.6W - 31.9W$. The maximum bubble size reached in tests of $\Delta t = 1.67s$ was $560.52\mu m$ with a power input of $28.551W$. In the set of tests $\Delta t = 28.2s$, the results were different, for a current equal to or larger than $2.2A$ the resistivity of the wire may have changed which provoked a variation in voltage measurements. This could represent a limitation of this strategy.

However, even with significantly low bubble sizes, it might still be possible for this approach to work. With the constant forming of bubbles on the wire, at a given liquid flow velocity, the drag force exerted on these bubbles needs to be lower than the surface tension force between bubble-wire until the bubbles reach a specific size. This specific size needs to be sufficient enough to able to aid in the atomization process, and also, the power necessary to produce these bubbles must not exceed the power utilized in the pressurization and injection of the gas applied in the current strategy of effervescent atomization, otherwise, this new strategy is redundant.

Future work

Employing only one thin wire to achieve a significant bubble generation seems to be implausible. It is imperative to change the approach of the hypothesis presented in this dissertation. Testing with multiple wires with different orientations, and longitudinal and axial locations is necessary to comprehend the viability of this concept. Moreover, the implementation of a bluff body, which will create a low-velocity recirculation zone, might be necessary in order to allow bubbles to be formed instead of their immediate collapse when subjected to a force exerted by a flowing liquid. Furthermore, it is worth pre-heating the liquid for comparison and to determine the morphology of bubbles produced in this case.

On another note, testing with degassed distilled water is required to guarantee that the bubbles formed where not only due to the existence of air inside the water.

Lastly, the variation of voltage measurements encountered requires further analysis in order to evaluate this occurrence.

Bibliography

O. Cejpek, M. Maly, V. K. Dhinasekaran, M. M. Avulapati, L. Dacanay, and J. Jedelsky. Novel atomizer concept for ccs applications: Impinging effervescent atomizer. *Separation and Purification Technology*, page 123259, 2023.

M. Ghazivini, M. Hafez, A. Ratanpara, and M. Kim. A review on correlations of bubble growth mechanisms and bubble dynamics parameters in nucleate boiling. *Journal of Thermal Analysis and Calorimetry*, pages 1–37, 2022.

T. Hibiki, H. Goda, S. Kim, M. Ishii, and J. Uhle. Structure of vertical downward bubbly flow. *International Journal of Heat and Mass Transfer*, 47(8-9):1847–1862, 2004.

H. Hu, C. Xu, Y. Zhao, K. J. Ziegler, and J. Chung. Boiling and quenching heat transfer advancement by nanoscale surface modification. *Scientific reports*, 7(1):1–16, 2017.

J. Jedelsky and M. Jicha. Energy conversion during effervescent atomization. *Fuel*, 111:836–844, 2013.

J. Jedelsky and M. Jicha. Energy considerations in spraying process of a spill-return pressure-swirl atomizer. *Applied energy*, 132:485–495, 2014.

I. Kang and L. Leal. The drag coefficient for a spherical bubble in a uniform streaming flow. *The Physics of fluids*, 31(2):233–237, 1988.

I. Kim, Y. Kamotani, and S. Ostrach. Modeling bubble and drop formation in flowing liquids in microgravity. *AIChE journal*, 40(1):19–28, 1994.

T. Kumada, H. Sakashita, and H. Yamagishi. Pool boiling heat transfer—i. measurement and semi-empirical relations of detachment frequencies of coalesced bubbles. *International journal of heat and mass transfer*, 38(6):969–977, 1995.

A. Lefebvre, X. Wang, and C. Martin. Spray characteristics of aerated-liquid pressure atomizers. *Journal of Propulsion and Power*, 4(4):293–298, 1988.

A. H. Lefebvre and V. G. McDonell. *Atomization and sprays*. CRC press, 2017.

D. W. Loebker and H. L. Empie Jr. High mass flowrate effervescent spraying of a high viscosity newtonian liquid. 1997.

J. Lu and X. Peng. Bubble slippage on thin wires during subcooled boiling. *International journal of heat and mass transfer*, 49(13-14):2337–2346, 2006.

J. Lu and X. Peng. Bubble oscillation on thin wire during subcooled boiling. *International journal of heat and mass transfer*, 51(17-18):4461–4469, 2008.

R. Marek and J. Straub. The origin of thermocapillary convection in subcooled nucleate pool boiling. *International Journal of Heat and Mass Transfer*, 44(3):619–632, 2001.

T. T. Nguyen, N. Tsuzuki, H. Murakawa, N. H. Duong, and H. Kikura. Measurement of the condensation rate of vapor bubbles rising upward in subcooled water by using two ultrasonic frequencies. *International Journal of Heat and Mass Transfer*, 99: 159–169, 2016.

S. Nukiyama. The maximum and minimum values of the heat q transmitted from metal to boiling water under atmospheric pressure. *International Journal of Heat and Mass Transfer*, 9(12):1419–1433, 1966.

M. O. Panão. Interpreting liquid atomization efficiency. *Int J Eng Tech & Inf*, 2(5): 121–124, 2021.

M. O. Panão, A. S. Moita, and A. L. Moreira. On the statistical characterization of sprays. *Applied Sciences*, 10(17):6122, 2020.

X. Pi and A. S. Rangwala. The influence of wire orientation during nucleate pool boiling in subcooled dodecane. *International Journal of Heat and Mass Transfer*, 137:1247–1257, 2019.

M. Rahman, M. Balzan, T. Heidrick, and B. Fleck. Effects of the gas phase molecular weight and bubble size on effervescent atomization. *International Journal of Multiphase Flow*, 38(1):35–52, 2012.

T. G. Shepard. *Bubble size effect on effervescent atomization*. University of Minnesota, 2011.

S. Sovani, P. Sojka, and A. Lefebvre. Effervescent atomization. *Progress in energy and combustion science*, 27(4):483–521, 2001.

W. Sowa. Interpreting mean drop diameters using distribution moments. *Atomization and Sprays*, 2(1), 1992.

J. Straub. Boiling heat transfer and bubble dynamics in microgravity. In *Advances in Heat Transfer*, volume 35, pages 57–172. Elsevier, 2001.

C. Sun, Z. Ning, X. Qiao, M. Lv, Y. Li, J. Zhao, and X. Wang. Measurements of internal flow regime and bubble size in effervescent atomizer. *Experimental Thermal and Fluid Science*, 98:604–620, 2018.

C. Sun, Z. Ning, X. Qiao, M. Lv, Y. Li, J. Zhao, and X. Wang. Study on effervescent spray morphology based on internal gas-liquid two-phase flow patterns. *European Journal of Mechanics-B/Fluids*, 74:123–138, 2019.

A. L. Thiebes, S. Klein, J. Zingsheim, G. H. Möller, S. Gürzing, M. A. Reddemann, M. Behbahani, S. Jockenhoevel, and C. G. Cornelissen. Effervescent atomizer as novel cell spray technology to decrease the gas-to-liquid ratio. *Pharmaceutics*, 14 (11):2421, 2022.

H. Wang, X. Peng, D. Christopher, W. Lin, and C. Pan. Investigation of bubble-top jet flow during subcooled boiling on wires. *International journal of heat and fluid flow*, 26(3):485–494, 2005.

H. Wang, X. Peng, S. V. Garimella, and D. M. Christopher. Microbubble return phenomena during subcooled boiling on small wires. *International Journal of Heat and Mass Transfer*, 50(1-2):163–172, 2007.

J. Wang, F.-C. Li, and X.-B. Li. Bubble explosion in pool boiling around a heated wire in surfactant solution. *International Journal of Heat and Mass Transfer*, 99: 569–575, 2016.

J. Xie, L. Liu, X. Liu, H. Qu, and R. Duan. Effect of bubble cutting on spray characteristics and dust control performance in the effervescent atomization. *Process Safety and Environmental Protection*, 167:493–499, 2022.

N. Xu, H. Jiang, L. Peng, D. Wang, and H. Chu. Dynamic analysis of bubble attachment and sweeping on microwire in subcooled nucleate pool boiling. *Journal of Thermal Science*, 30:1842–1858, 2021.

N. Young, J. S. Goldstein, and M. Block. The motion of bubbles in a vertical temperature gradient. *Journal of Fluid Mechanics*, 6(3):350–356, 1959.

F. Zhao, Z. Ren, B. Xu, H. Zhang, and C. Fu. Brief overview of effervescent atomizer application. In *Journal of Physics: Conference Series*, volume 1300, page 012043. IOP Publishing, 2019.

J. Zhao, G. Liu, S. Wan, and N. Yan. Bubble dynamics in nucleate pool boiling on thin wires in microgravity. *Microgravity Science and Technology*, 20:81–89, 2008.

Appendix A. Additional Data and Designs

Bubble generation frequency

A visual count of bubbles released from the wire was done for test times of t=[8.7s; 28.2 s; 84.6s] considering small bubbles ($50\mu m < D_b < 100\mu m$), and larger bubbles around the same size or larger than the wire ($D_b \geq 100\mu m$). While the algorithm developed in Matlab could correctly identify bubbles in the wire and those released with good contrast in the camera's field of view, smaller bubbles (focused or unfocused) would require further development of the algorithm, which one proposes as future work. Therefore, the following analysis is qualitative.

Table A.1 presents the number of focused and unfocused departed bubbles counted for input power values (P) between 13.29 W and 23.25 W. Tests in the interval $P \in [17.20; 18.56]$ W show a slight difference in bubble count resulting from a small time apart between tests, as well as different test time intervals. Namely, Tests 1 to 4: $\Delta t = 28.6\ s$; and Tests 5 to 8: $\Delta t = 8.7\ s$.

		Small Bubbles		Bubbles	
Test	P [W]	Focused	Unfocused	Focused	Unfocused
1	13.29	13+	30+	27	3
2	14.53	20+	26+	38	27
3	15.88	10+	35+	11	13
4	17.20	7+	14+	3	11
5	18.56	16+	10+	6	7
6	20.19	9+	14+	5	4+
7	21.65	6+	13+	4	4
8	23.25	5+	7+	N/A	2

Table A.1: Visual bubble departure count Tests with $\Delta t = 8.7s$ and $\Delta t = 28.6s$. (8 different power input)

Micro bubble regime only occurred in the final moments of this set of experiments from test 4 to 8 (in Table A.1), and considering it micro bubble regime might not be appropriate since it was observed a significant yet low micro bubble count (lower count for lower power supplies).

Table A.2 exhibits another set of test of the same analysis in experiments of around $\Delta t = 84.6s$.

		Small Bubbles		Bubbles	
Test	P [W]	Focused	Unfocused	Focused	Unfocused
1	14.81	36+	35+	64	20
2	16.07	52+	46+	62	17
3	17.65	60+	61+	61	29
4	18.91	19+	16+	23	18
5	20.45	9+	9+	13	20
6	22.02	23+	27+	8	12
7	23.87	19+	18+	5	7
8	25.73	-	-	-	-

Table A.2: Visual bubble departure count Tests with $\Delta t = 84.6s$. (8 different power input)

After Test 8 (in Table A.2) it proved to be extremely difficult and trivial to count departed bubbles of significant size, since most collapsed from start to finish. However micro bubble regime was reached with the exception of Test 1. In this set it was safe to assume a developed micro bubble regime after less than 31 seconds for power input of 31.95W. And, although longer for lower power, it was also reached after at least 54 seconds.

In the figure that follows one can see the micro bubble regime reached.

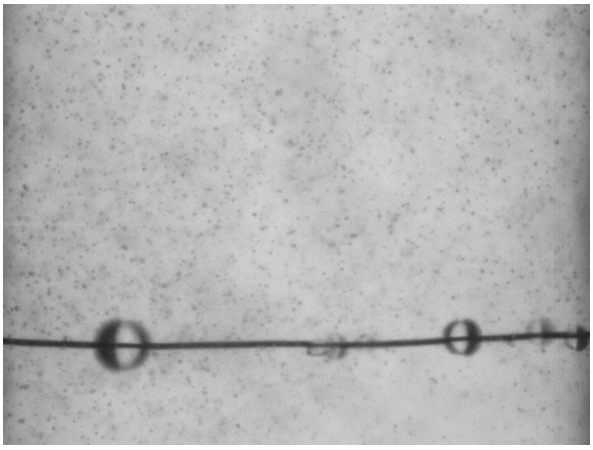

Figure A.1: Micro bubble regime reached with $P = 31.95W$ after 31s.

Given the considerable low bubble count compared to the tests time, the focus of determining bubble departure diameter, size distribution and velocity shifted to analysing bubble size and growth velocity on the wire. And it was mostly focused on the first stages of boiling.

Experimental apparatus design

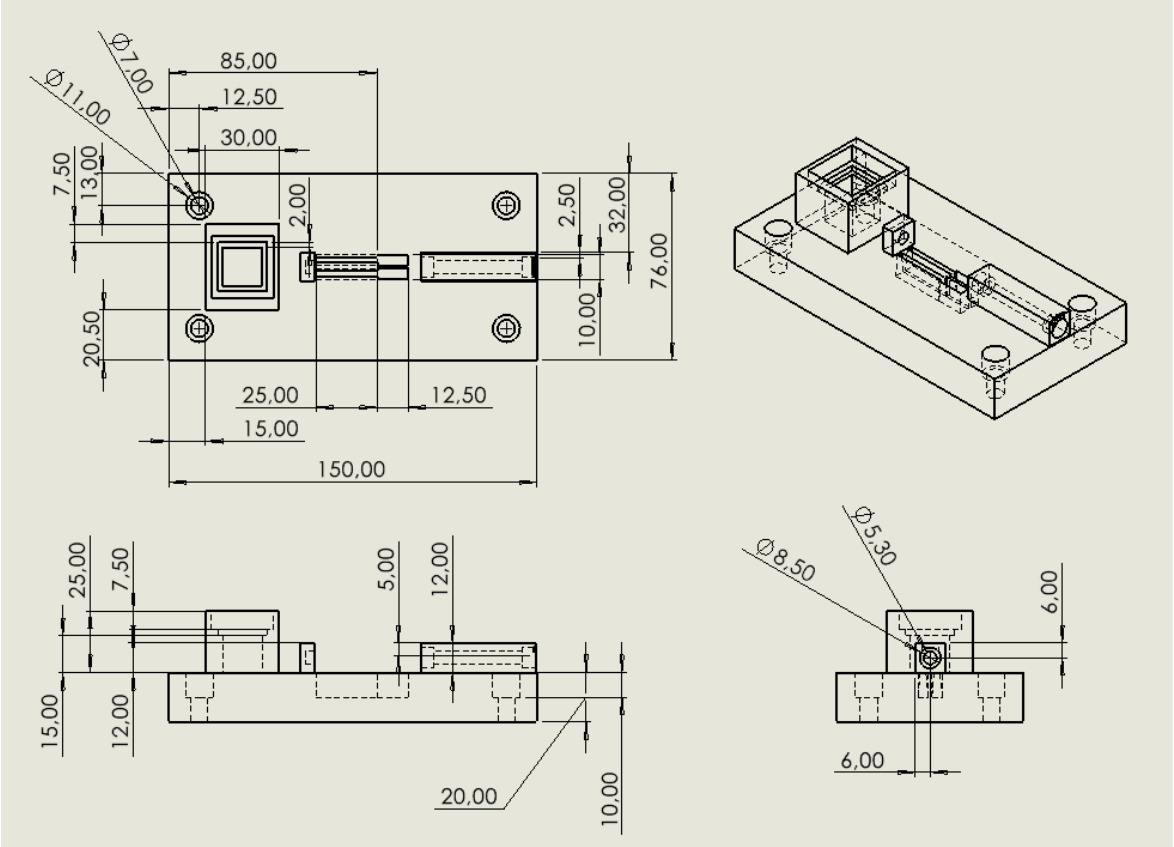

Figure A.2: Base design - Solidworks.

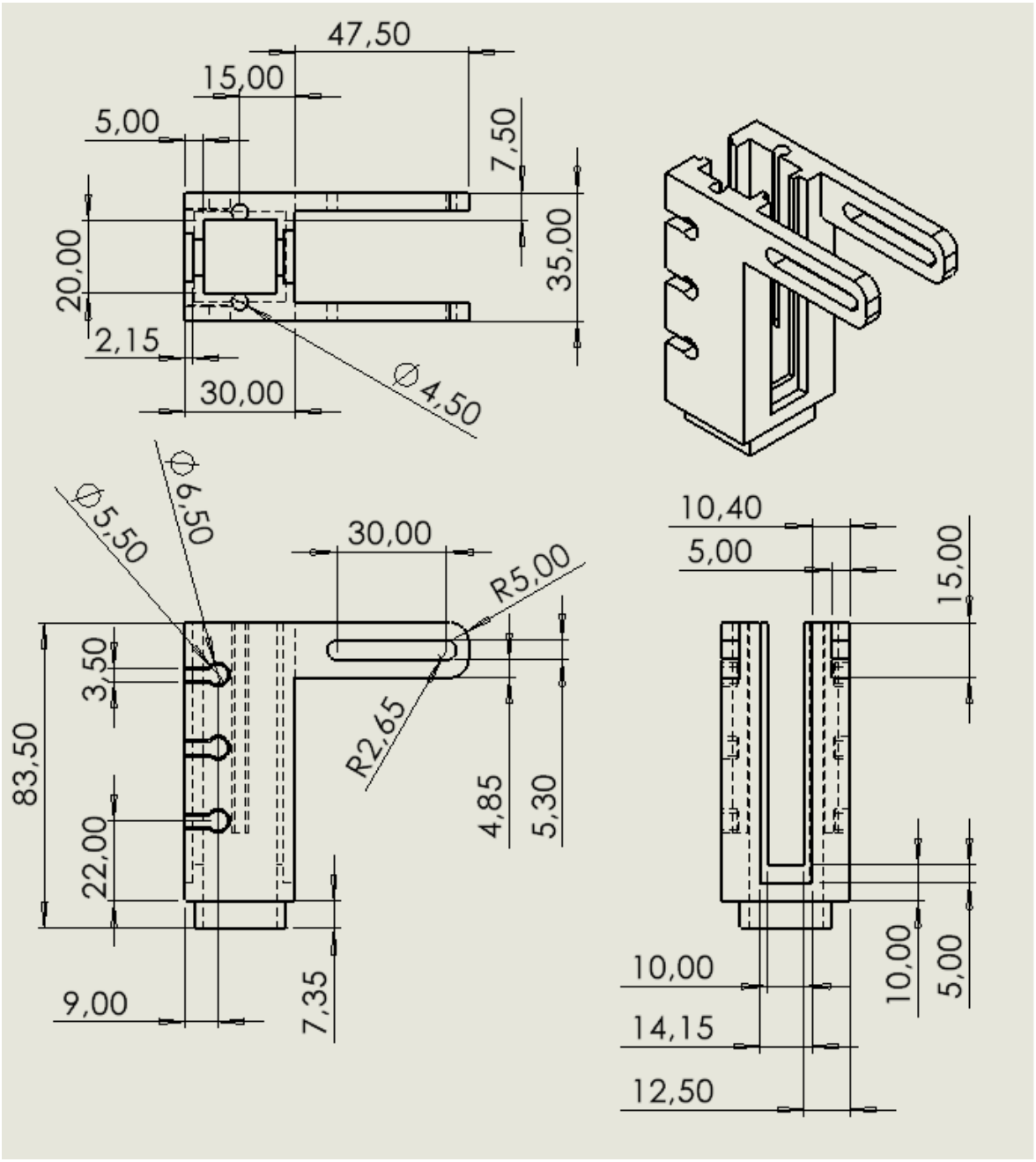

Figure A.3: Top Part design - Solidworks.

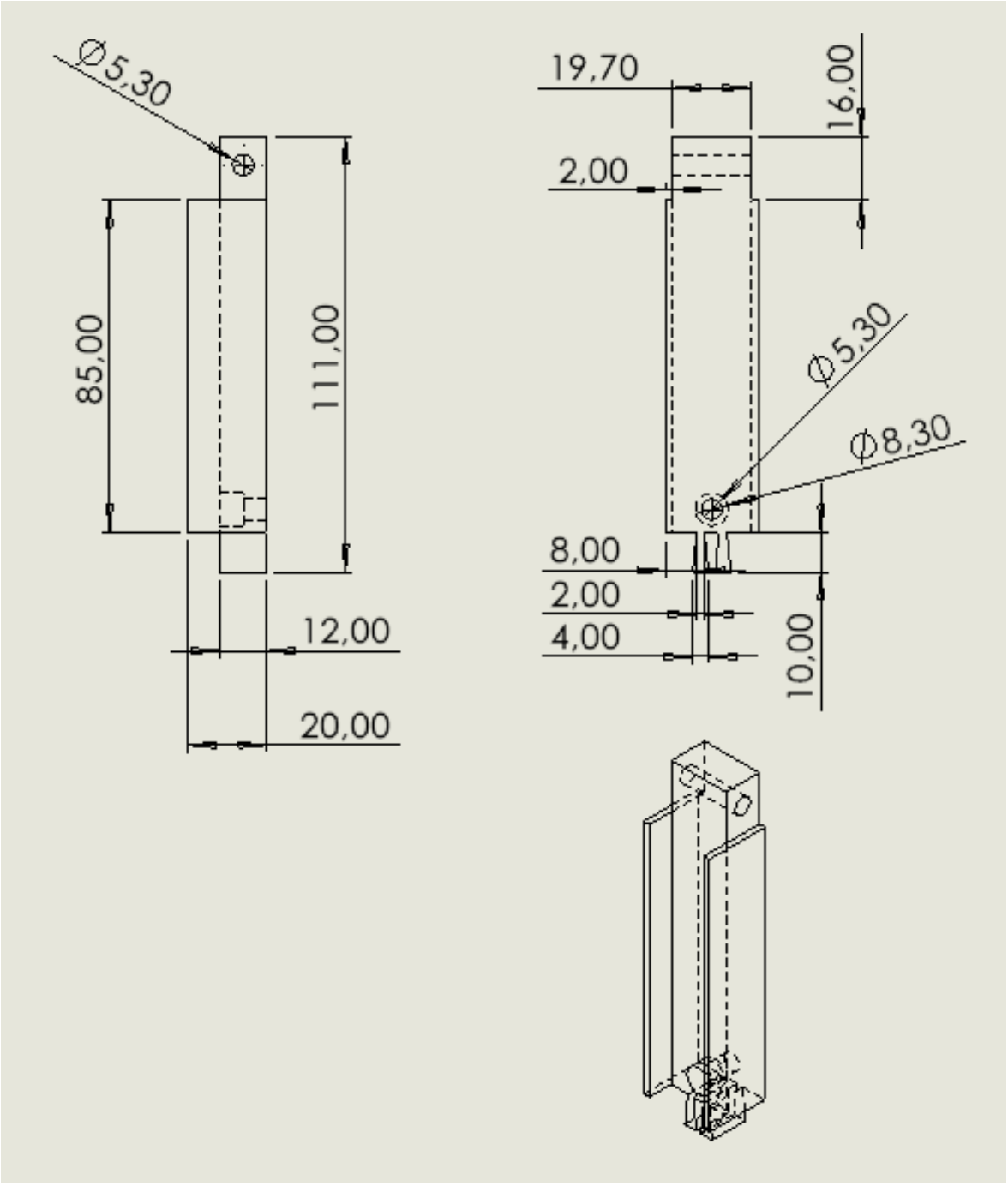

Figure A.4: LED's Support design - Solidworks.